Supplementary Information

Spatial Imaging of Carbon Reactivity Centers in Pd/C Catalytic Systems

Evgeniy O. Pentsak,[1] Alexey S. Kashin,[1] Mikhail V. Polynski[1,2], Kristina Kvashnina,[3] Pieter Glatzel[3] and Valentine P. Ananikov[1,4*]

[1] *Zelinsky Institute of Organic Chemistry, Russian Academy of Sciences, Leninsky Prospect 47, Moscow, 119991, Russia. E-mail: val@ioc.ac.ru*

[2] *MSU, Faculty of Chemistry, GSP-1, 1-3 Leninskiye Gory, Moscow 1, 119991, Russia*

[3] *ESRF - The European Synchrotron, 71 avenue des Martyrs, 38000 Grenoble, France*

[4] *Department of Chemistry, Saint Petersburg State University, Stary Petergof, 198504, Russia*

1. Spatial imaging of different types of defects by Pd nanoparticles

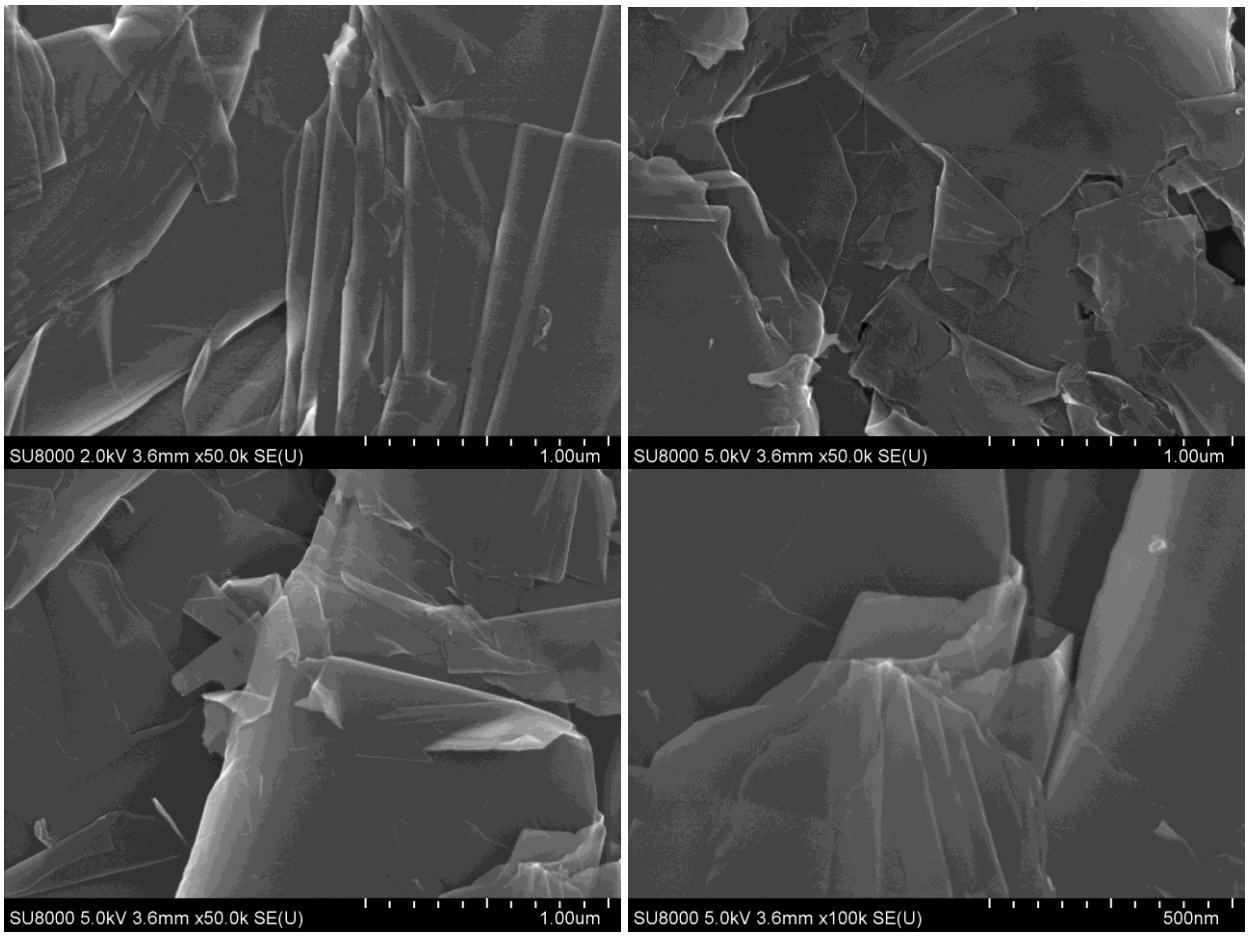

Figure S1. Initial carbon material (before attachment of Pd particles).

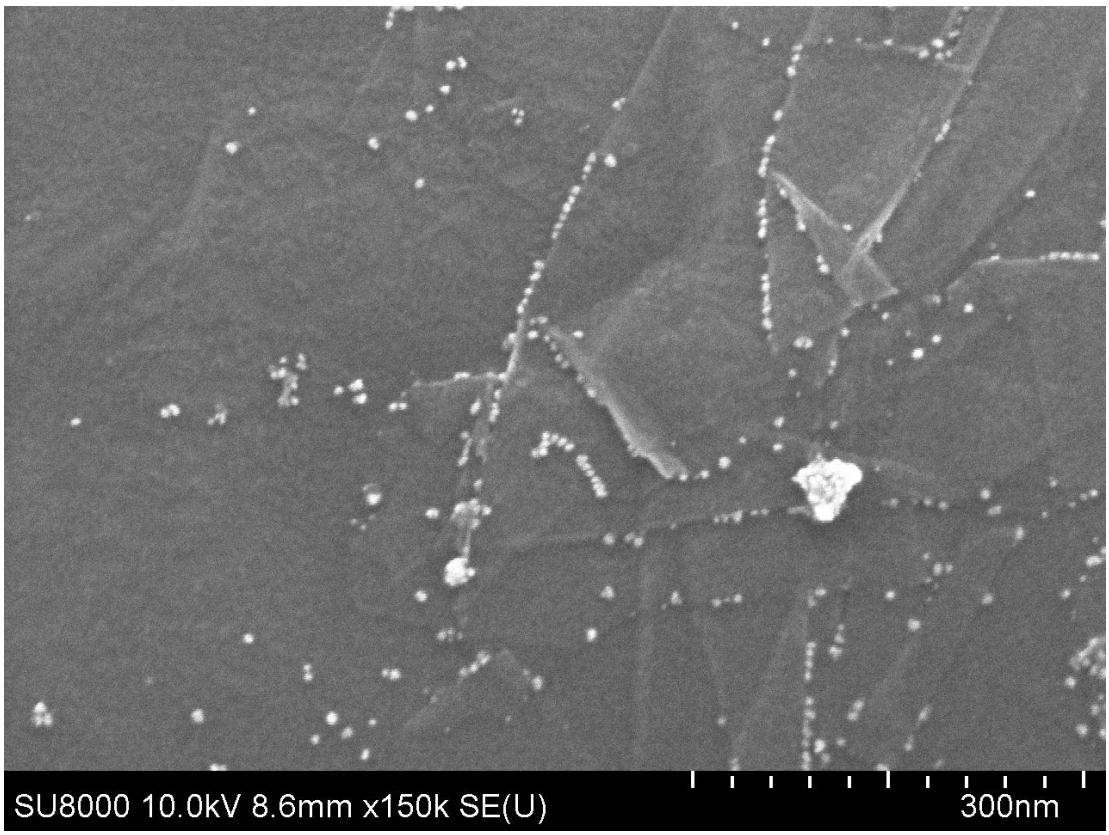

Figure S2. Enlarged image of the figure 3.

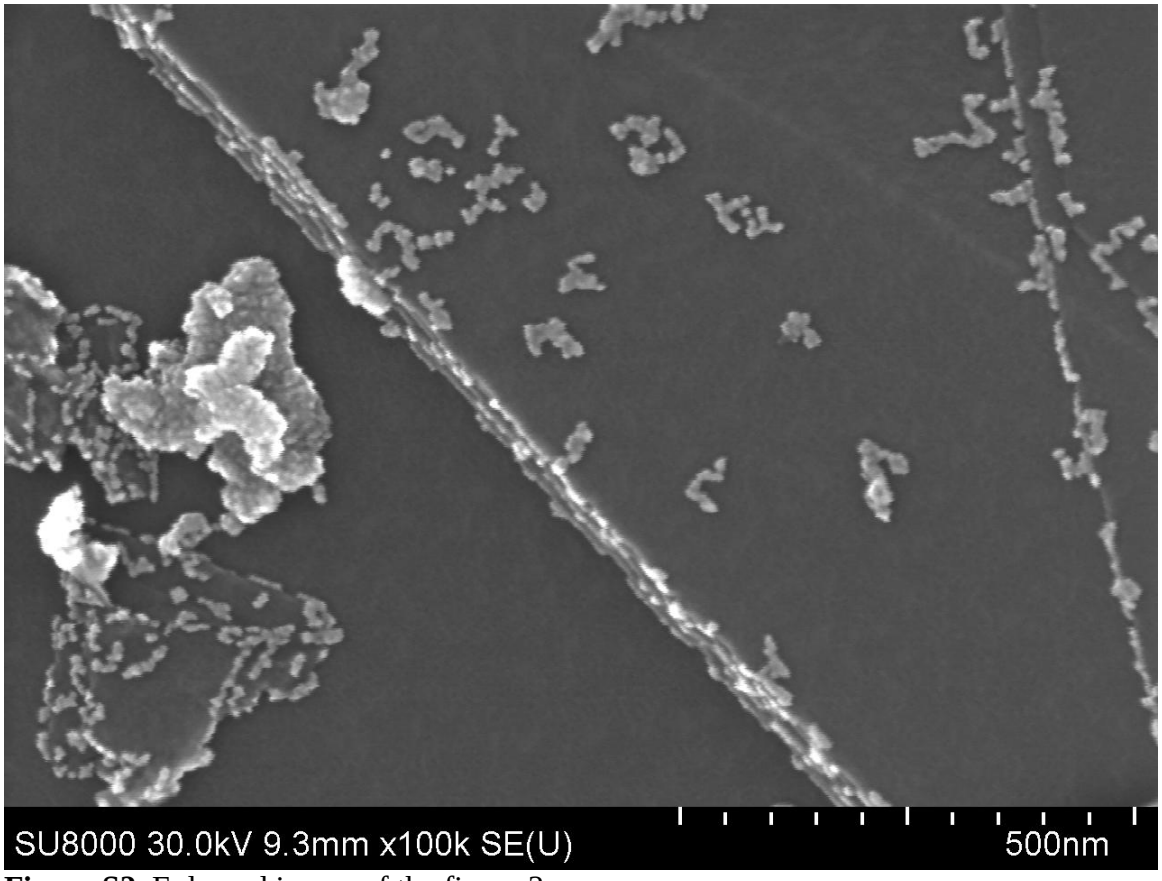

Figure S2. Enlarged image of the figure 3.

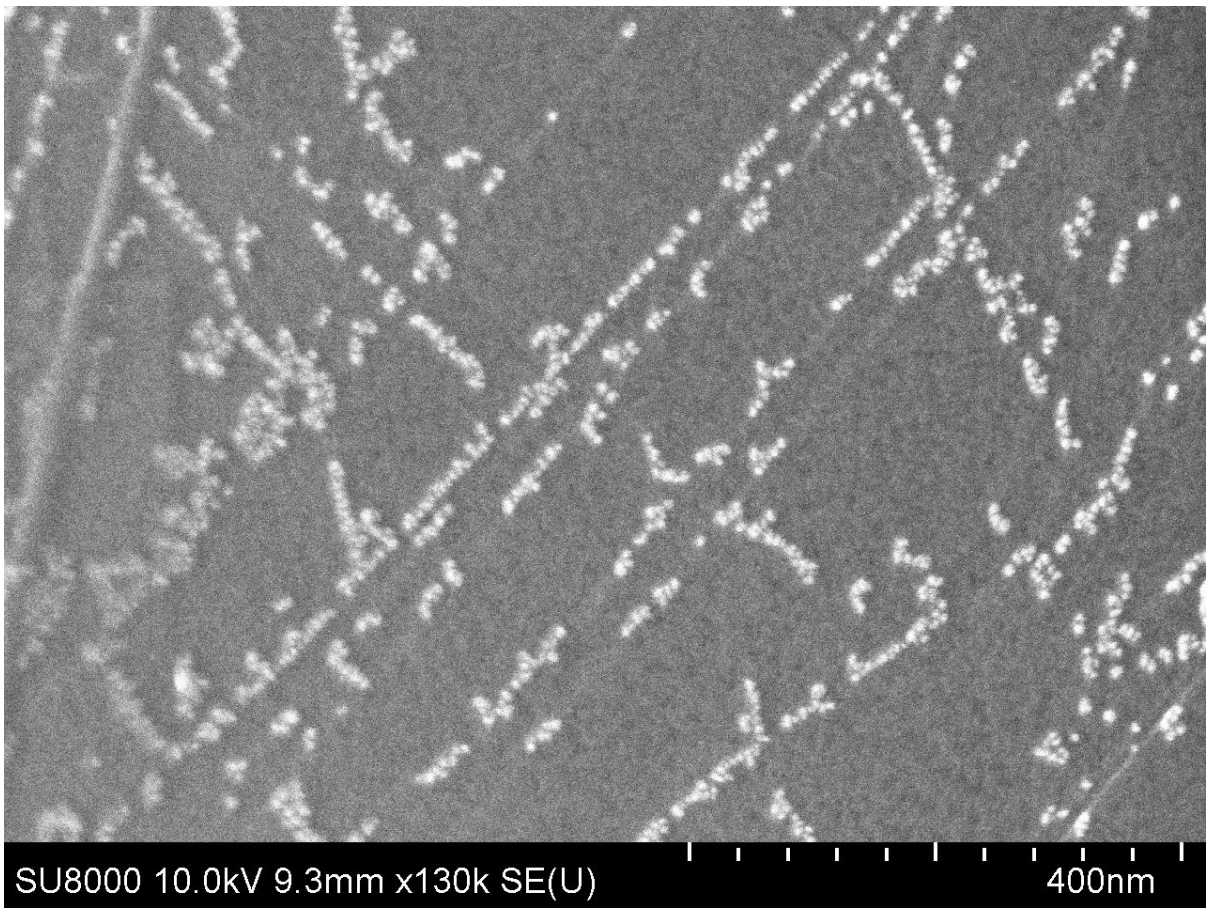

Figure S3. Enlarged image of the figure 3.

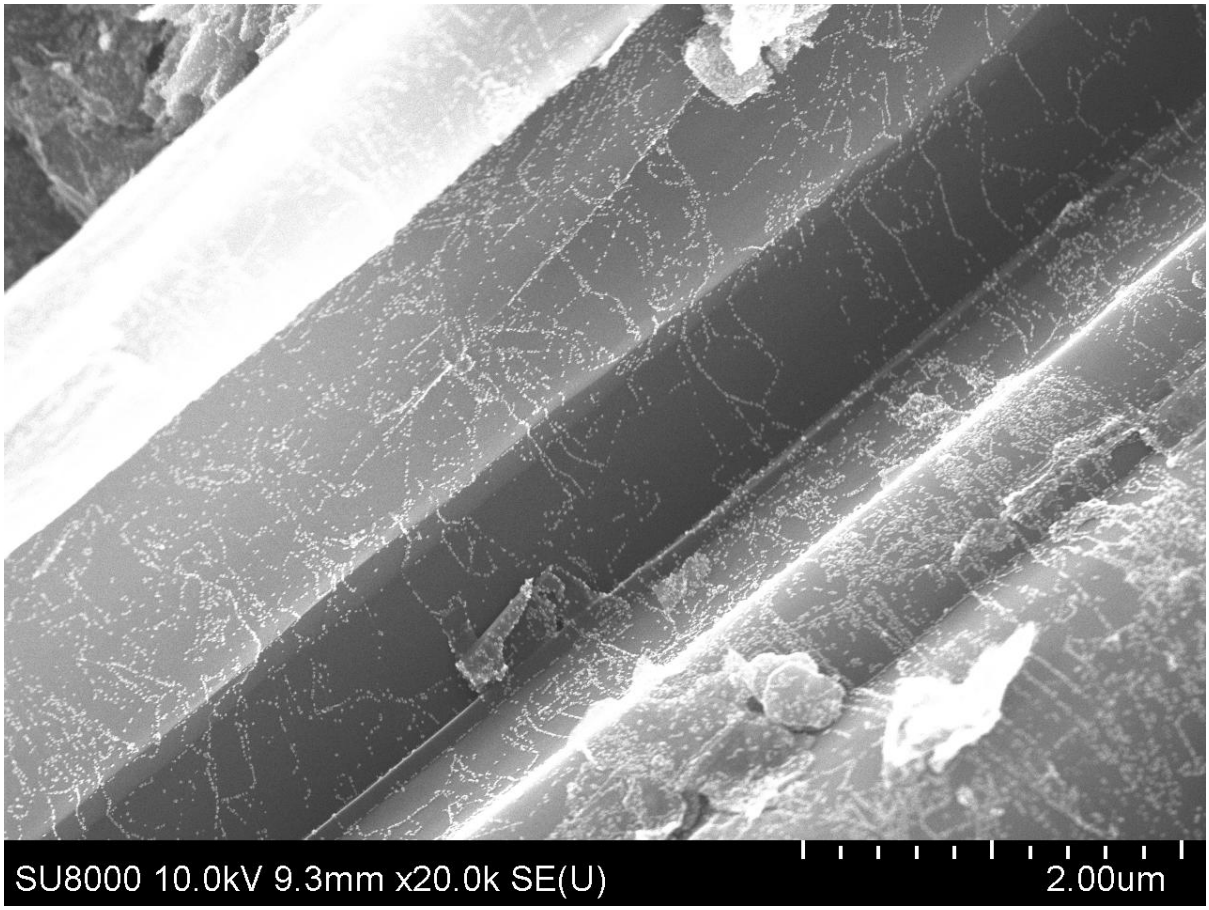

Figure S4. Enlarged image of the figure 3.

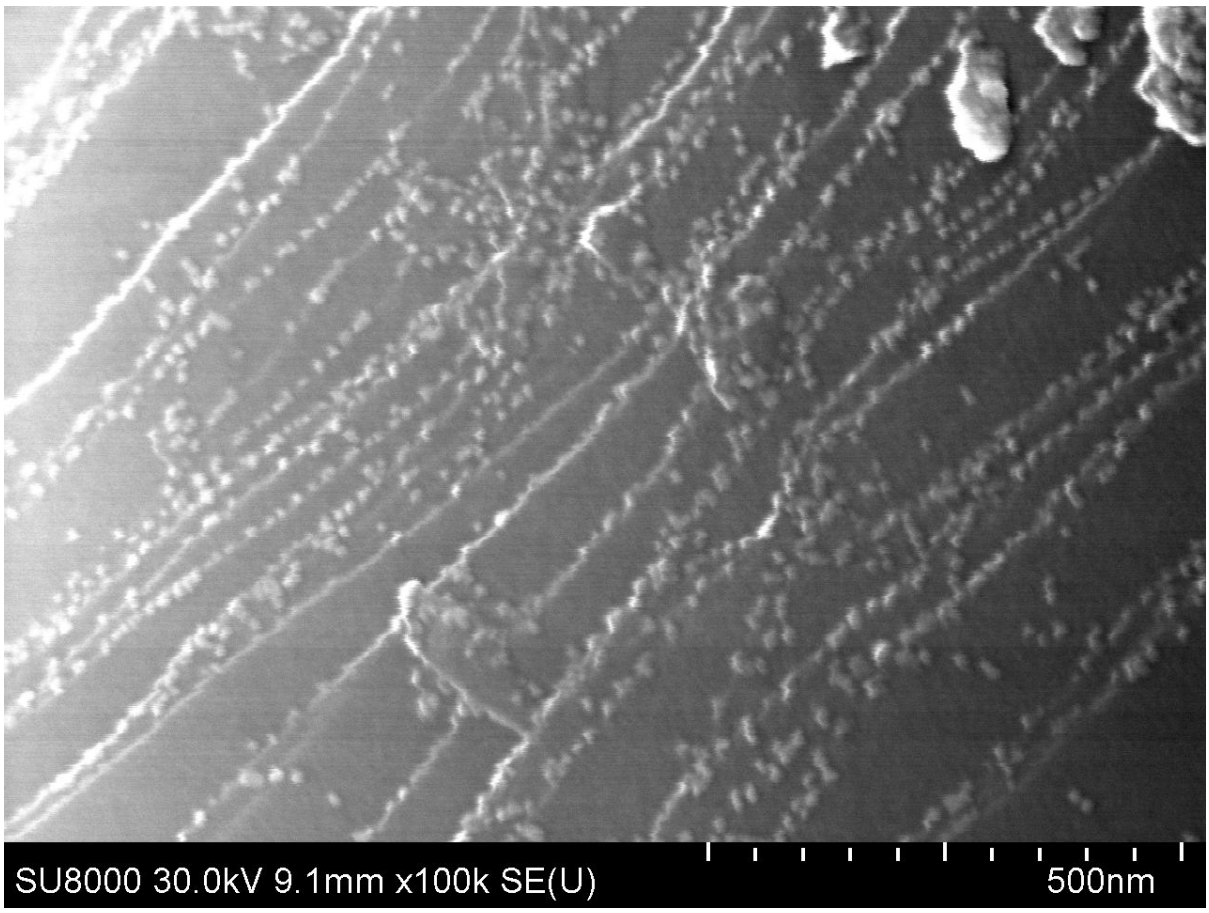

Figure S5. Enlarged image of the figure 3.

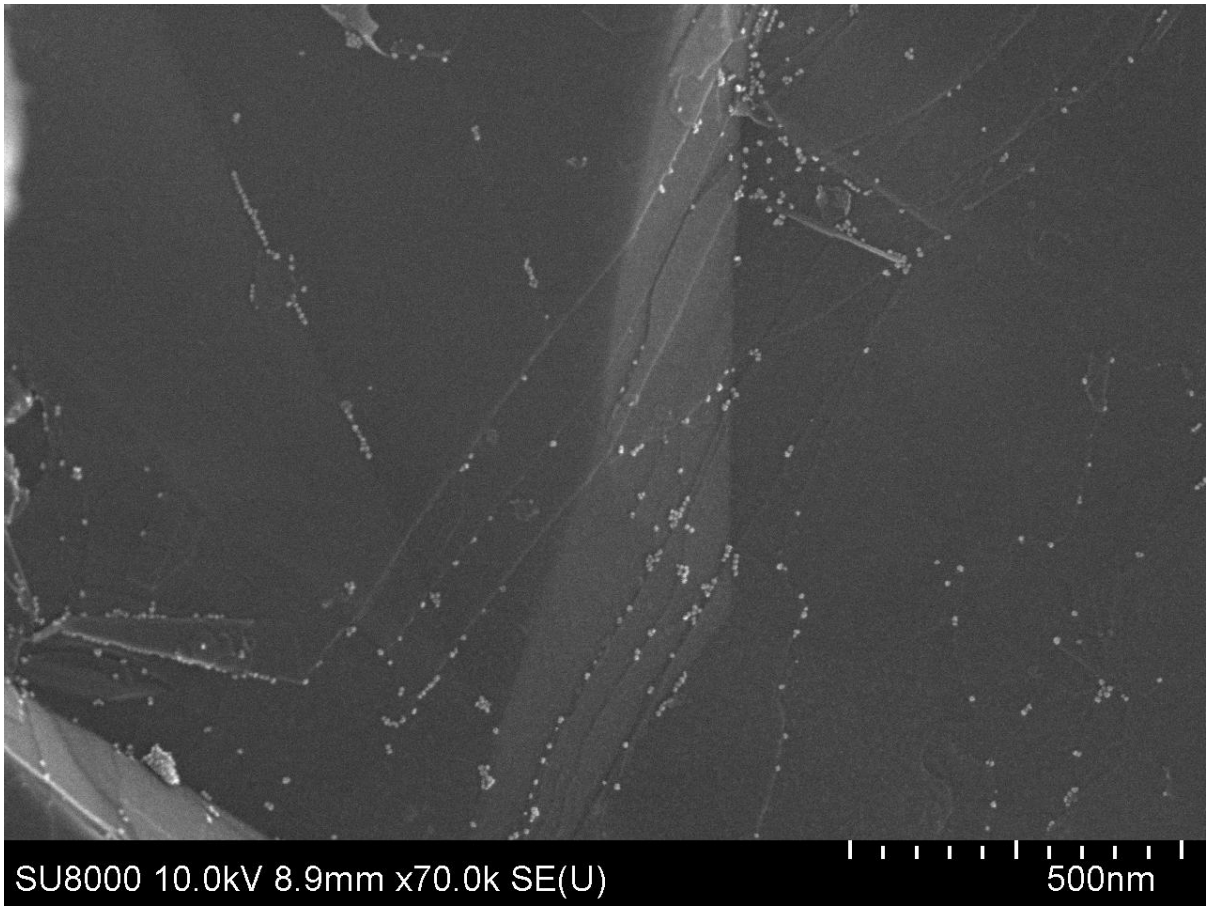

Figure S6. Enlarged image of the figure 3.

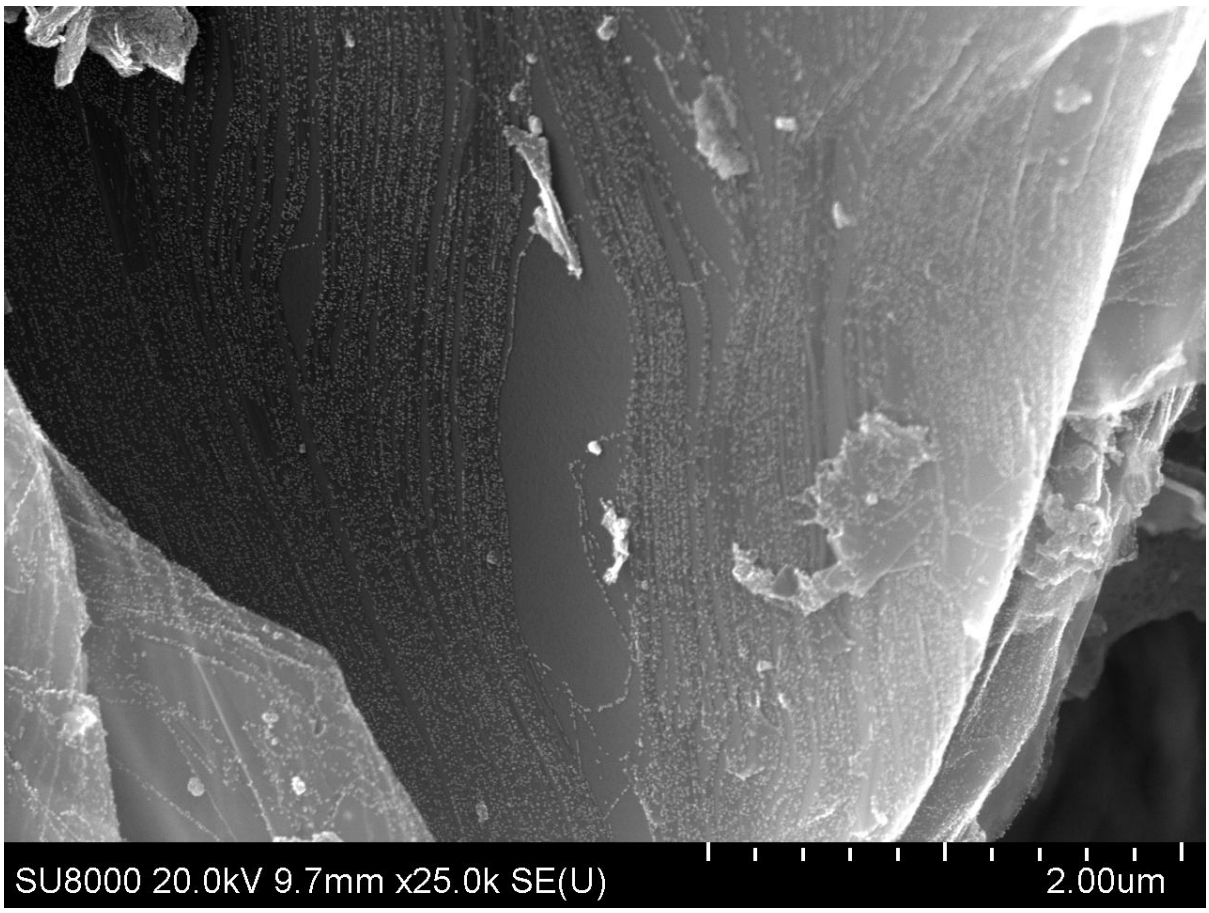

Figure S7. FE-SEM-image of defects mapped by Pd NPs.

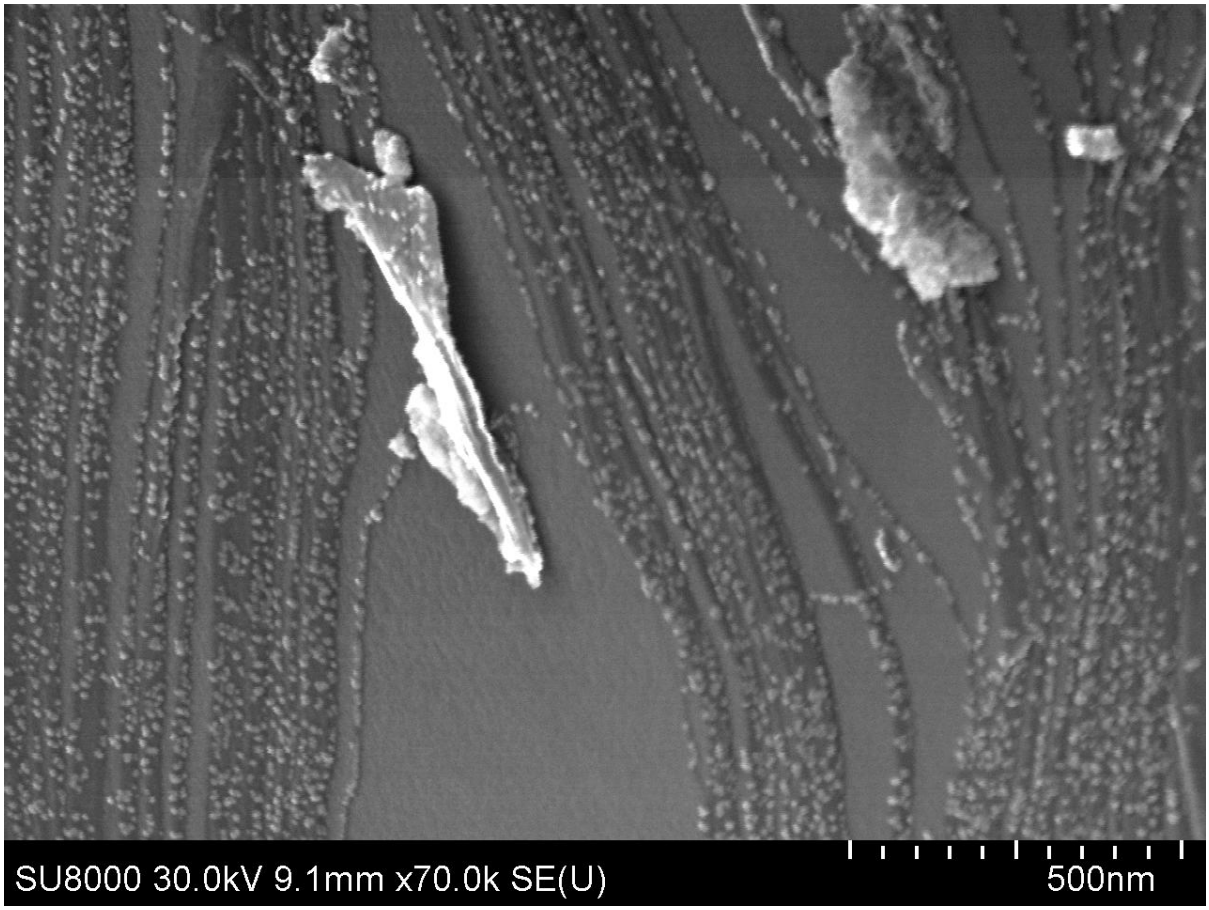

Figure S8. FE-SEM-image of defects mapped by Pd NPs.

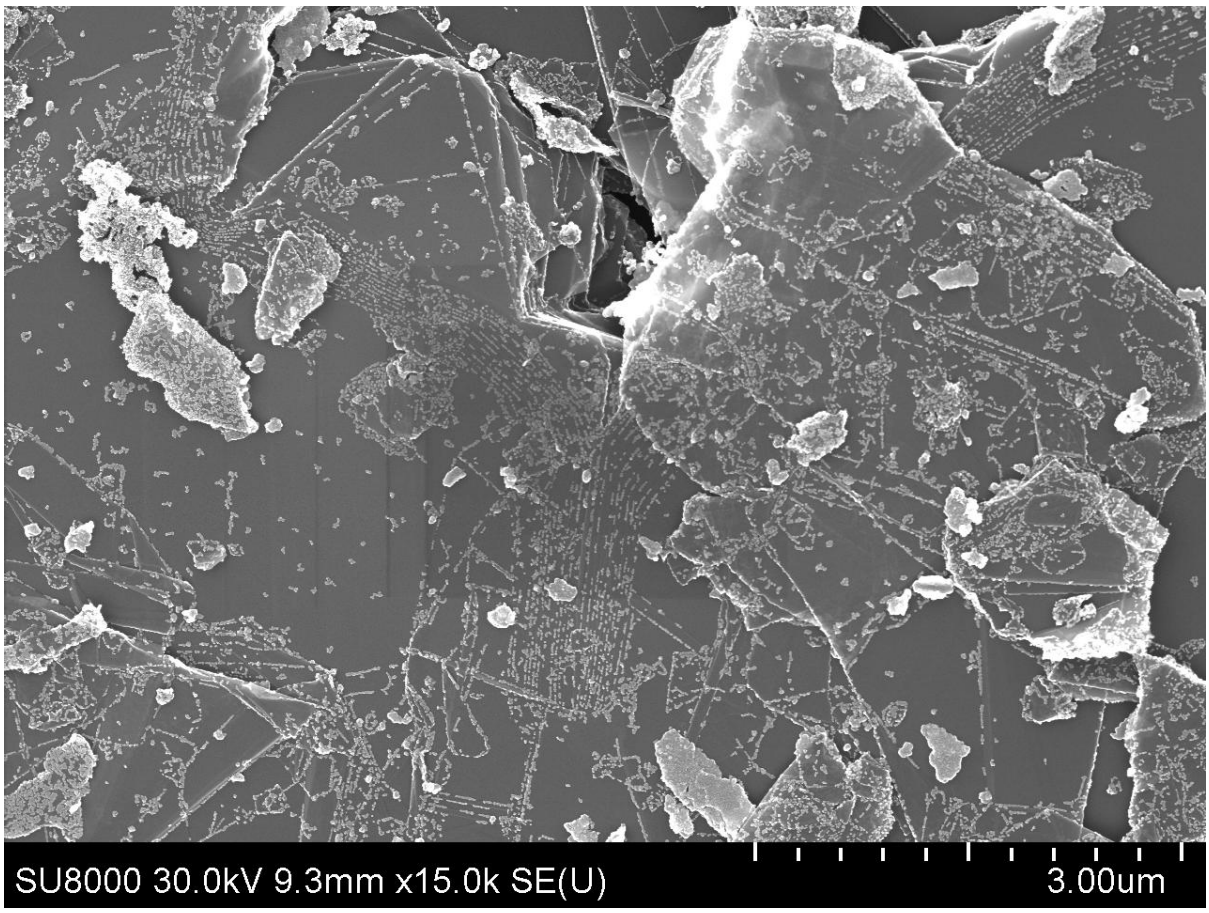

Figure S9. FE-SEM-image of defects mapped by Pd NPs.

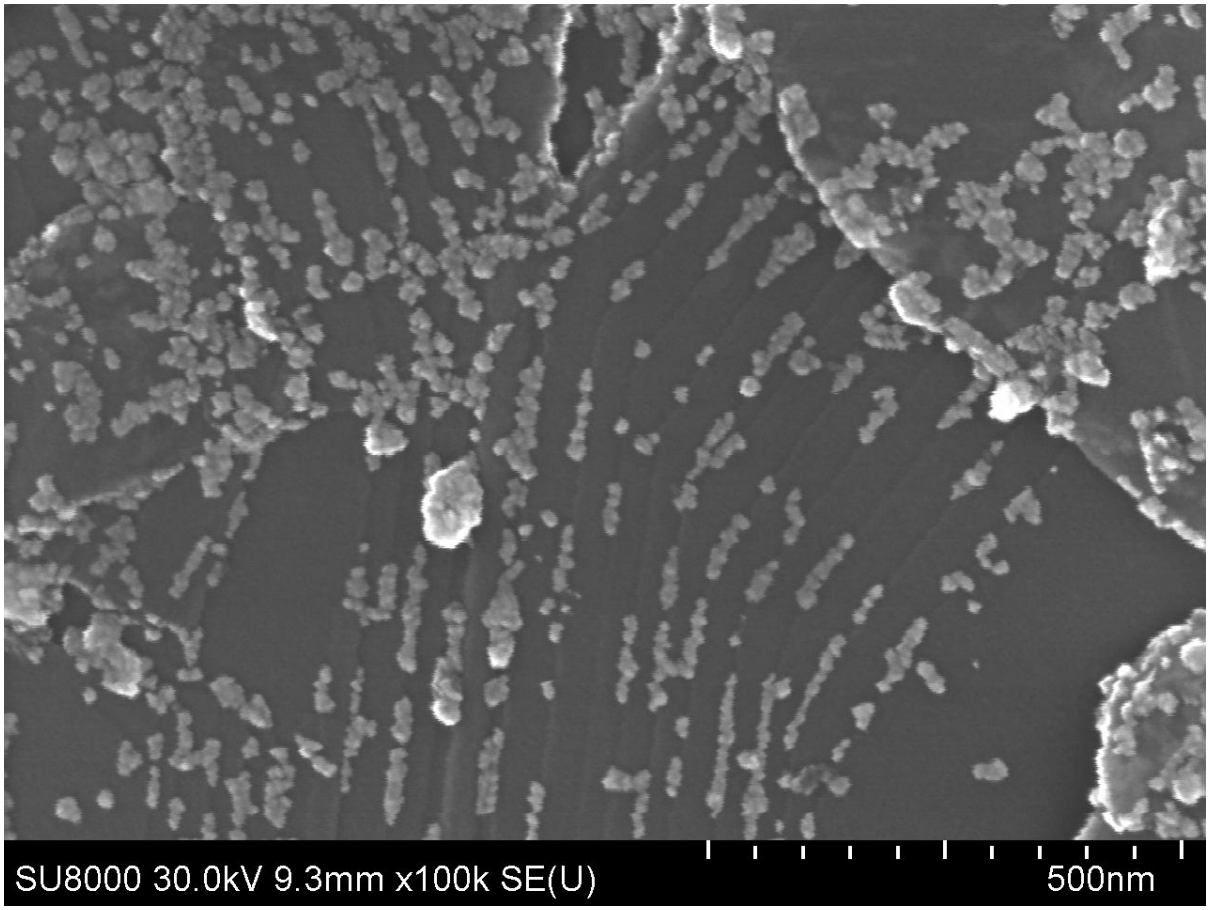

Figure S10. FE-SEM-image of defects mapped by Pd NPs.

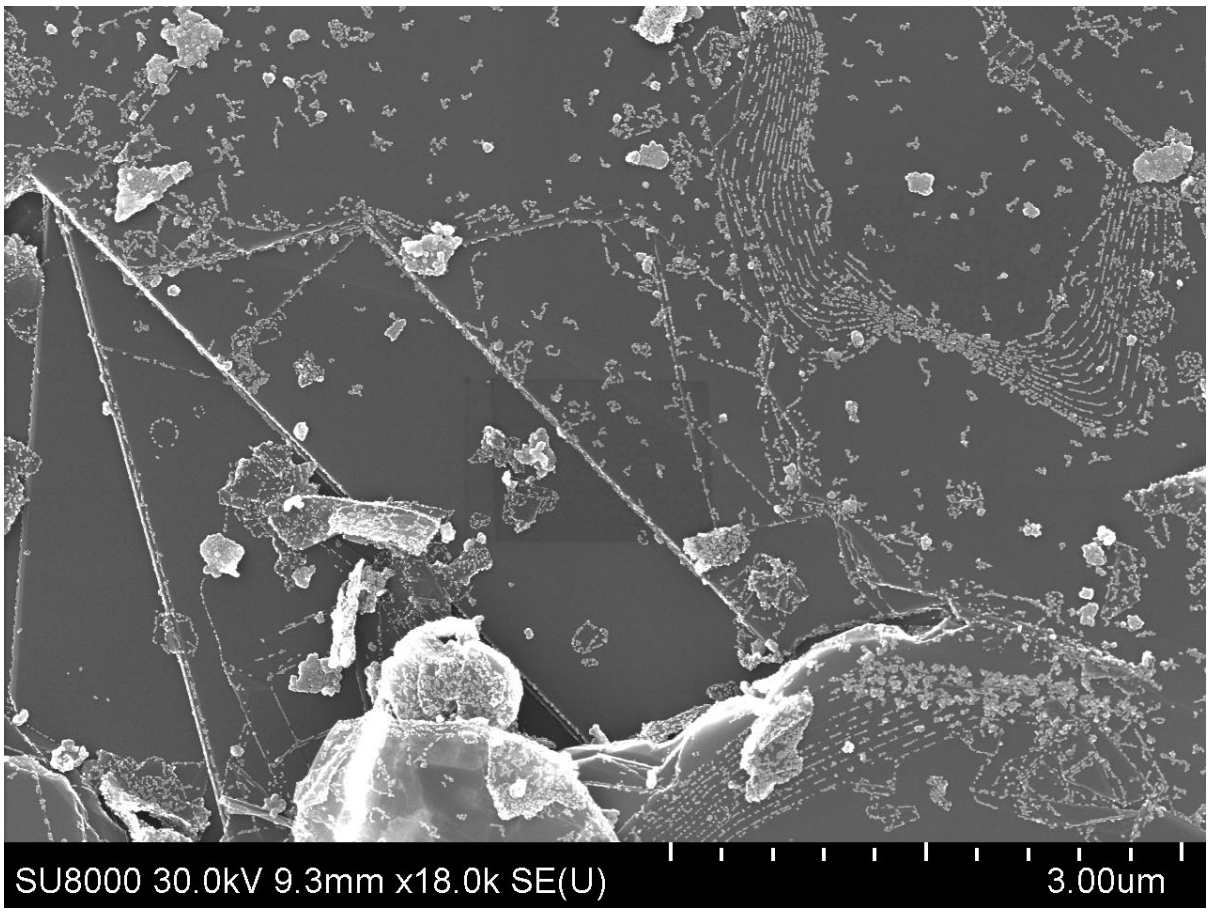

Figure S11. FE-SEM-image of defects mapped by Pd NPs.

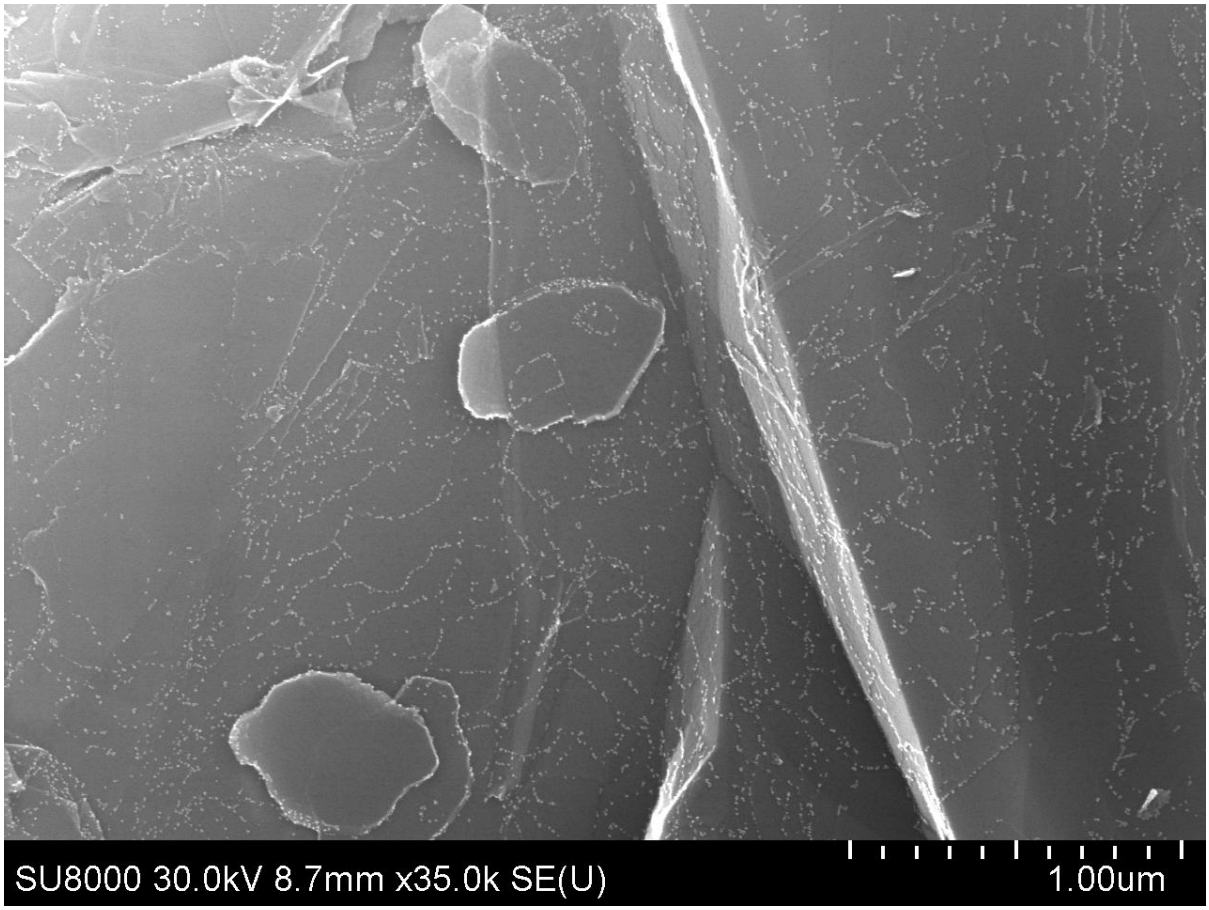

Figure S12. FE-SEM-image of defects mapped by Pd NPs.

Figure S13. FE-SEM-image of defects mapped by Pd NPs.

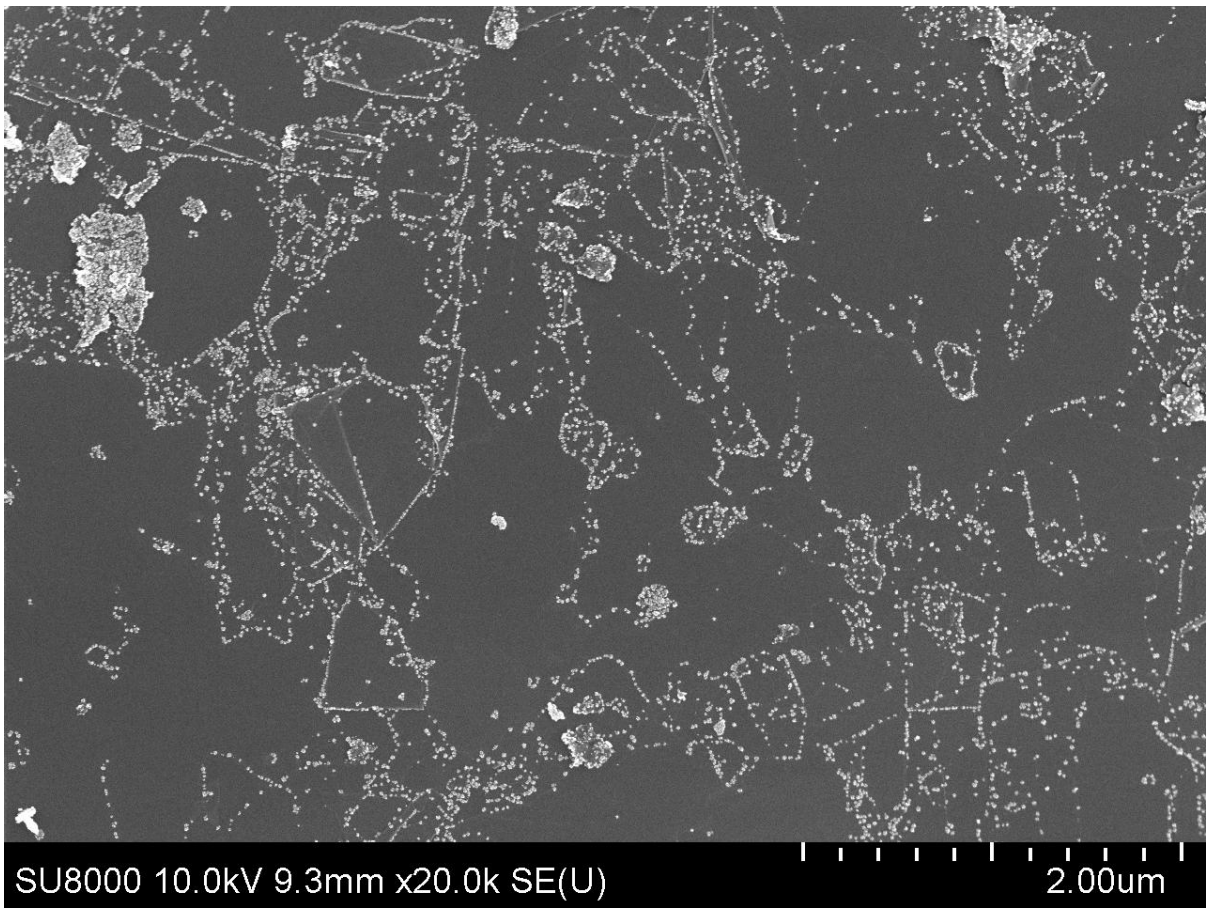

Figure S14. FE-SEM-image of defects mapped by Pd NPs.

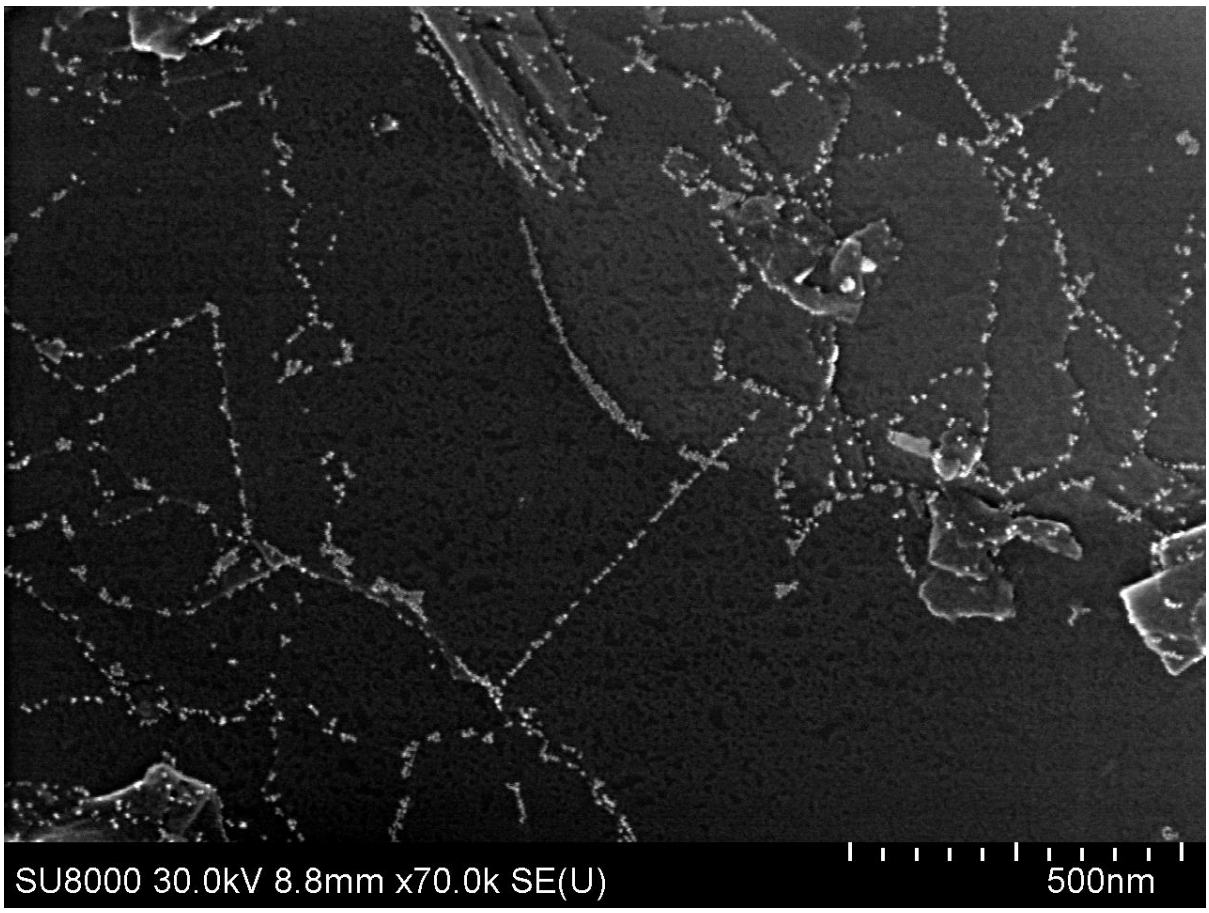

Figure S15. FE-SEM-image of defects mapped by Pd NPs.

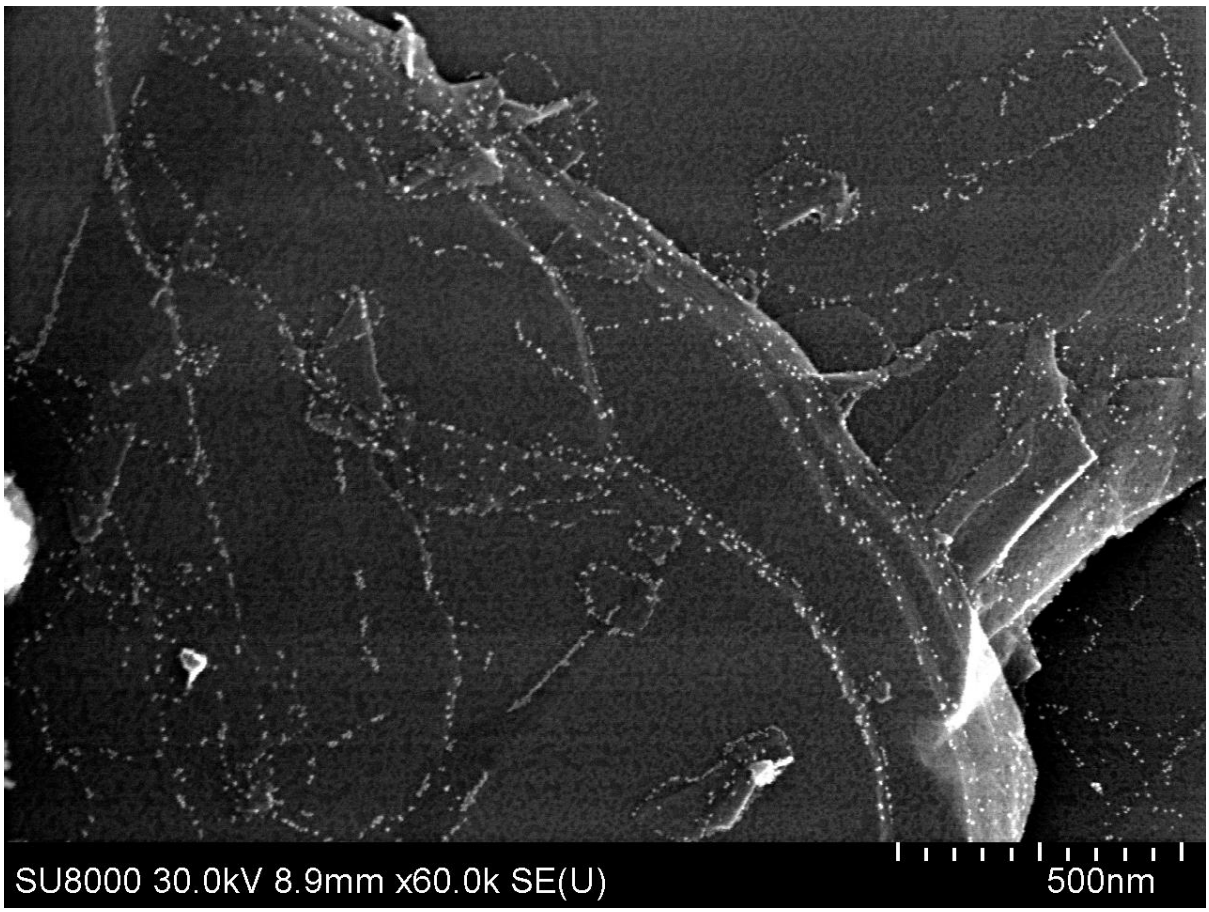

Figure S16. FE-SEM-image of defects mapped by Pd NPs.

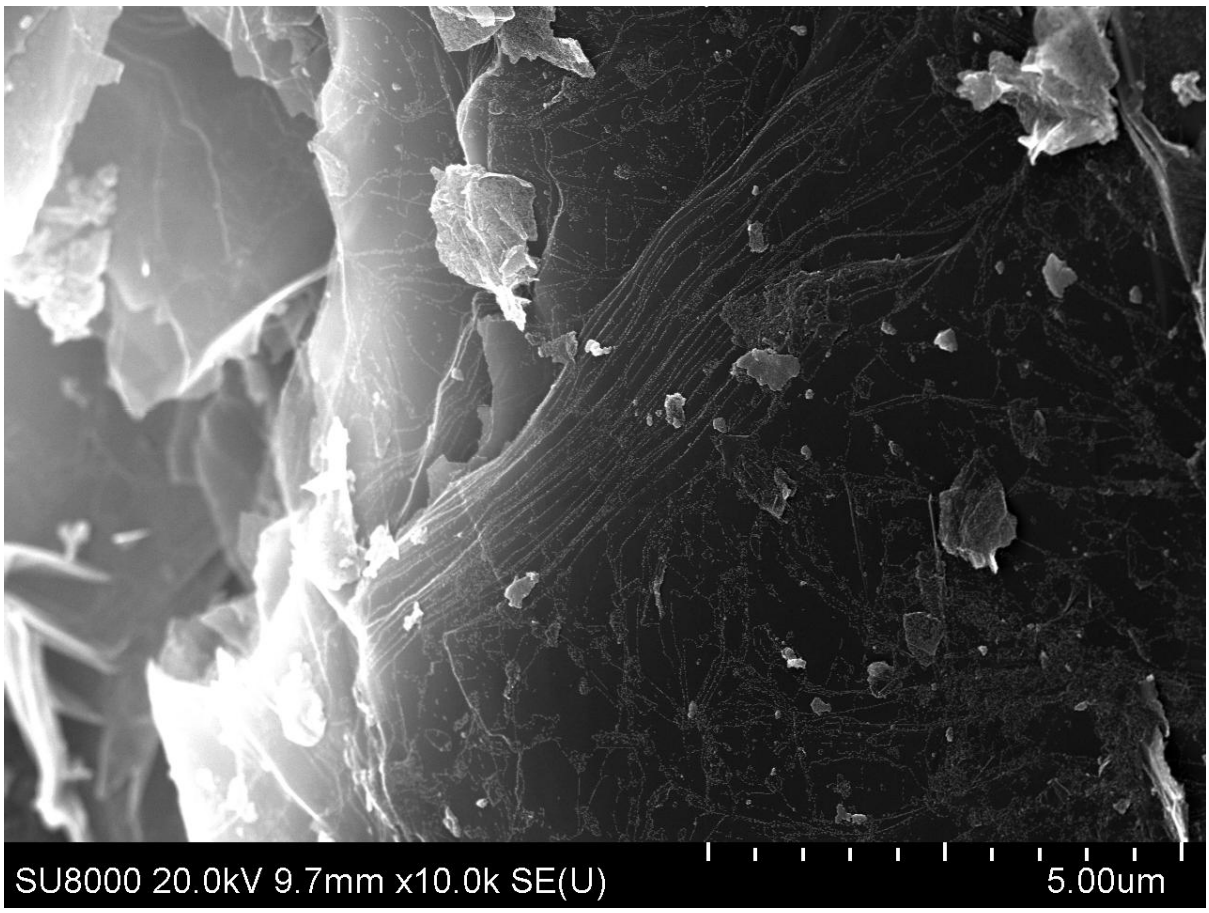

Figure S17. FE-SEM-image of defects mapped by Pd NPs.

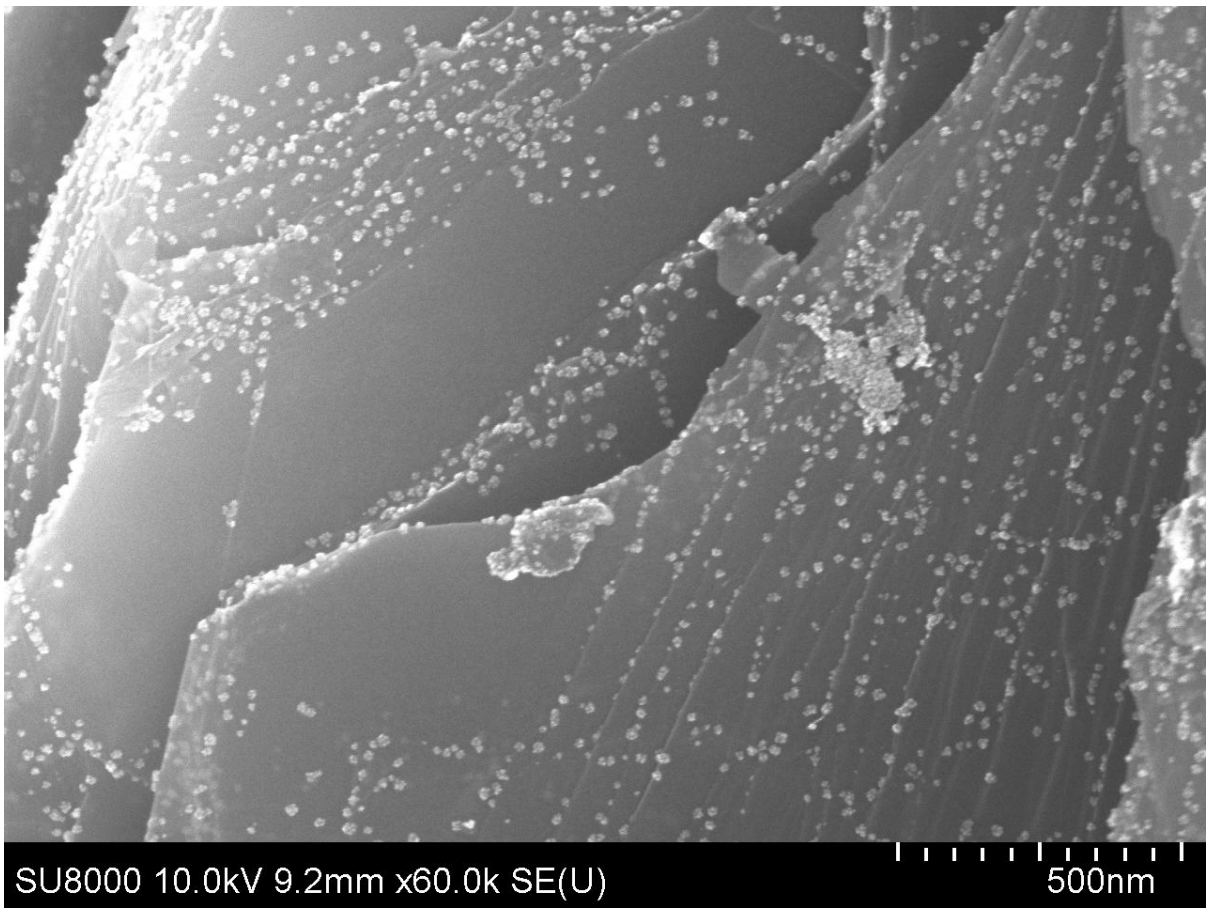

Figure S18. FE-SEM-image of defects mapped by Pd NPs.

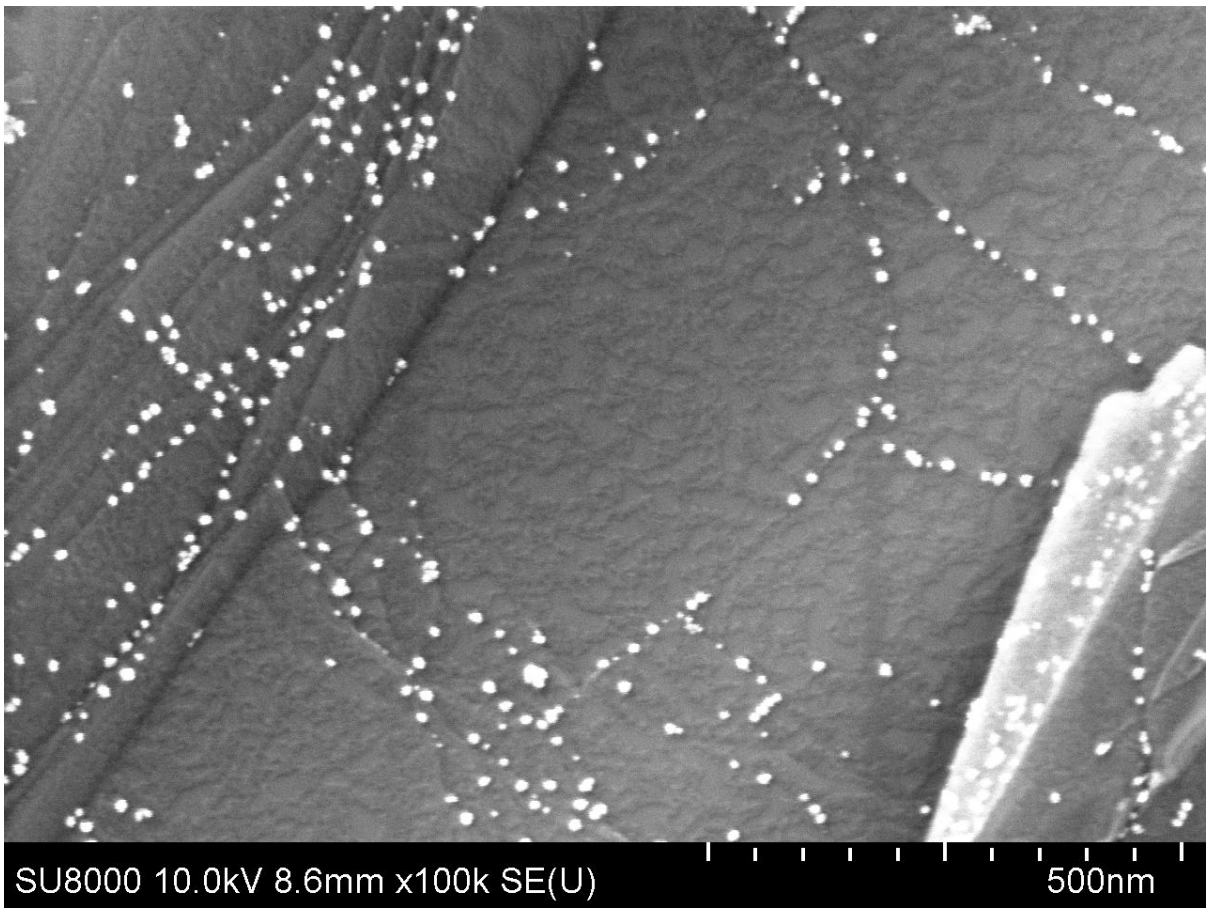

Figure S19. FE-SEM-image of defects mapped by Pd NPs.

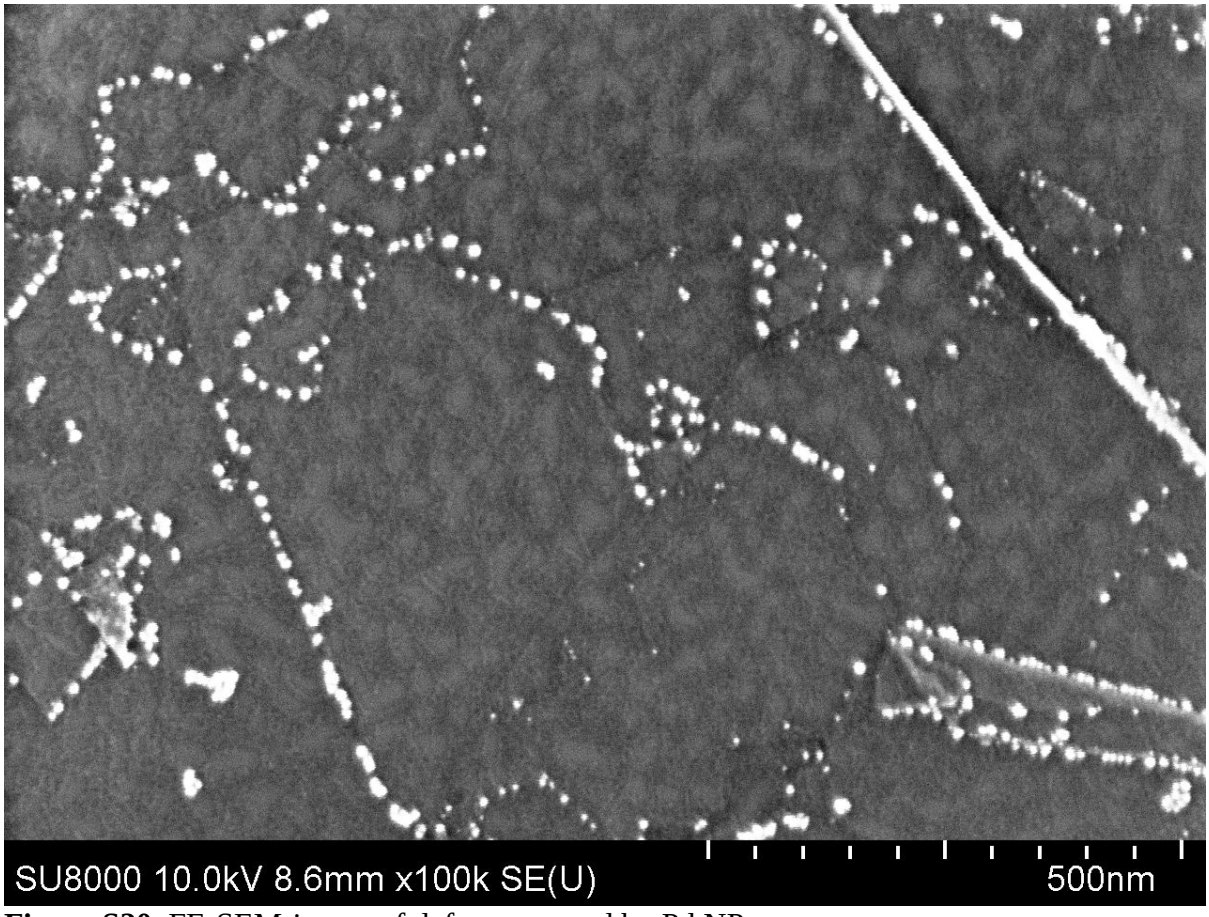

Figure S20. FE-SEM-image of defects mapped by Pd NPs.

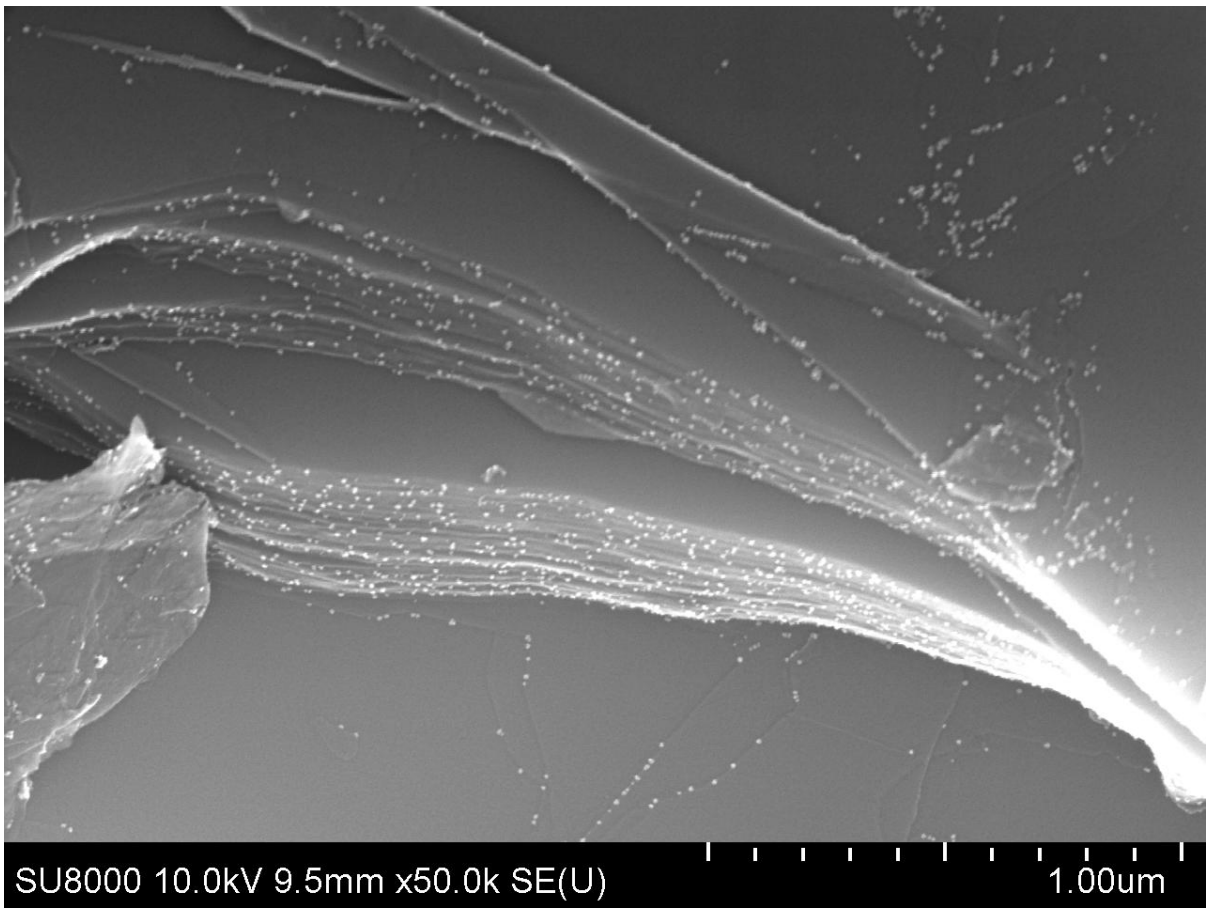

Figure S21. FE-SEM-image of defects mapped by Pd NPs.

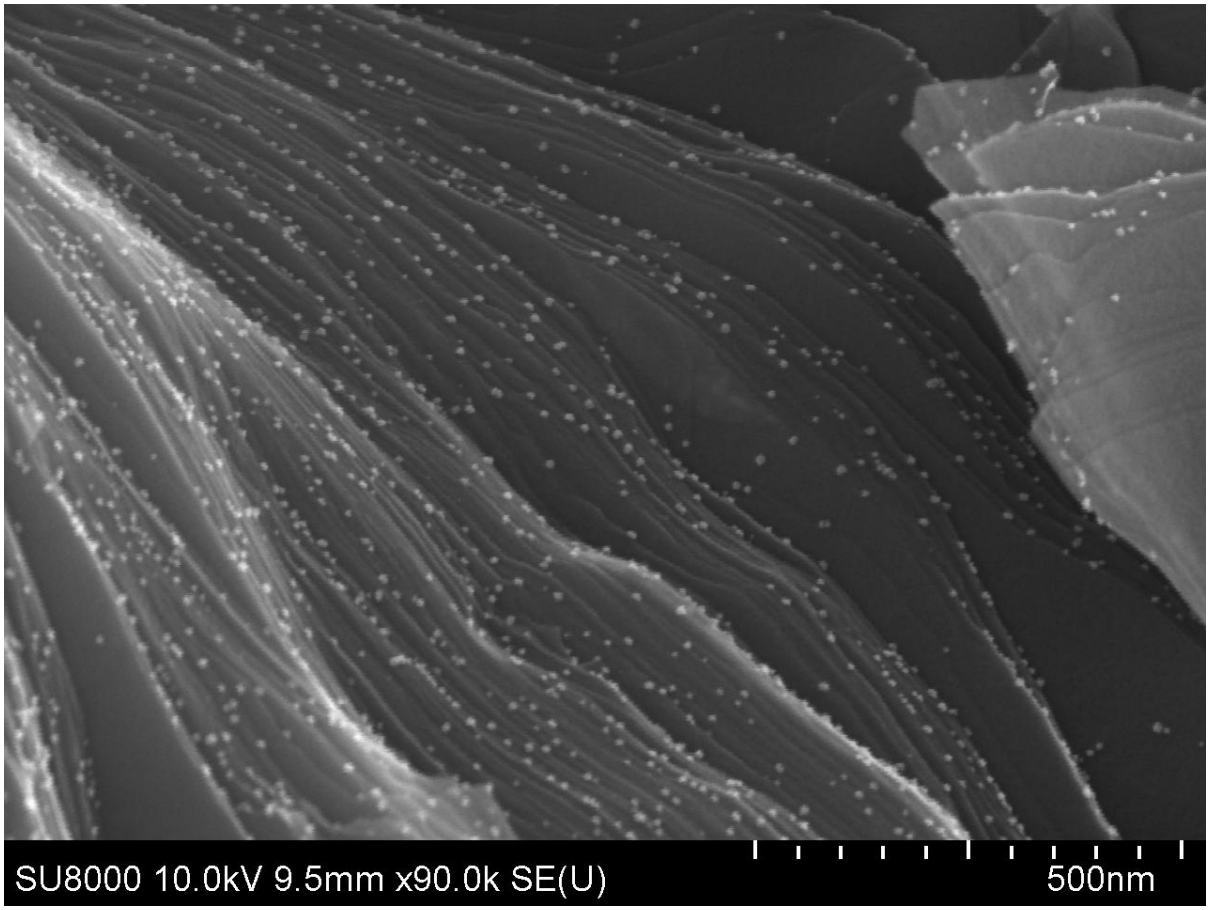

Figure S22. FE-SEM-image of defects mapped by Pd NPs.

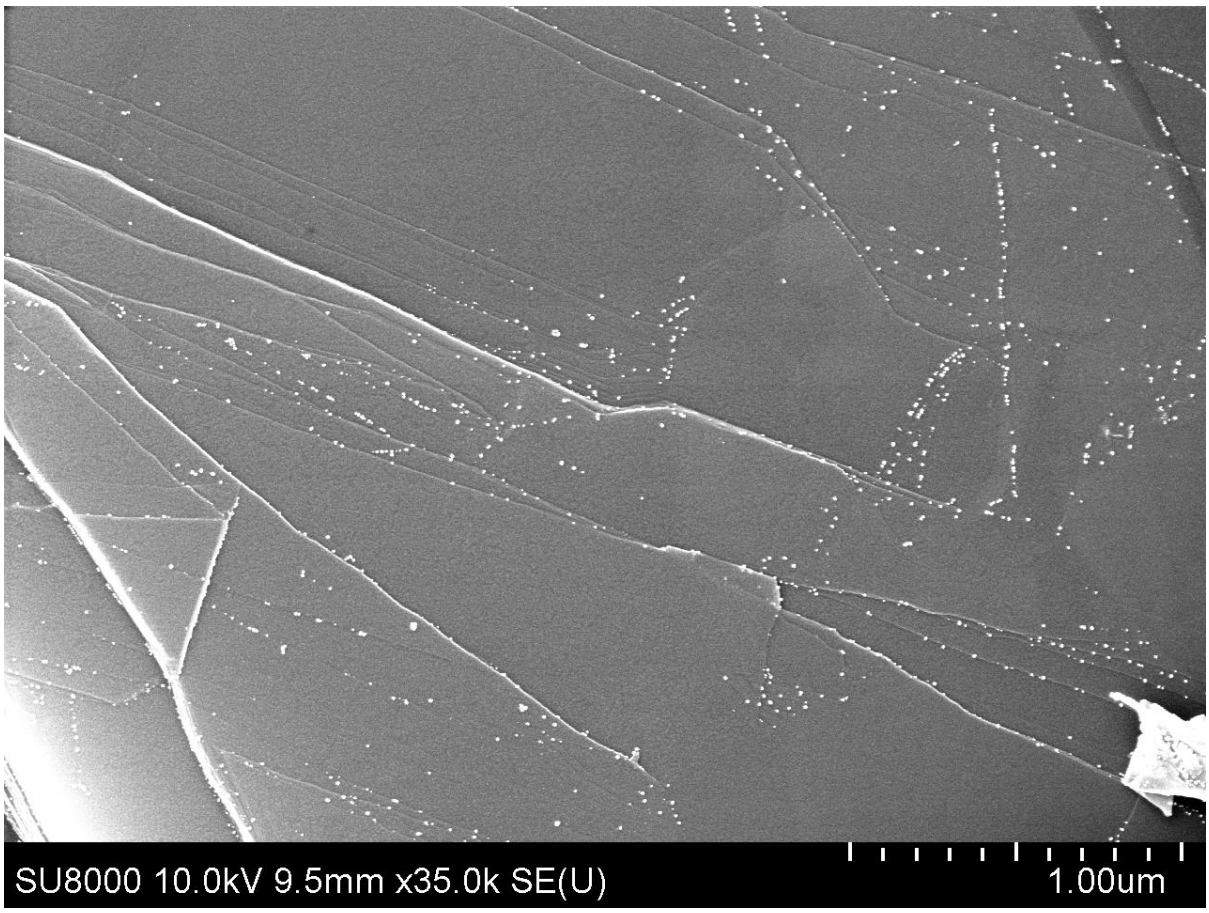

Figure S23. FE-SEM-image of defects mapped by Pd NPs.

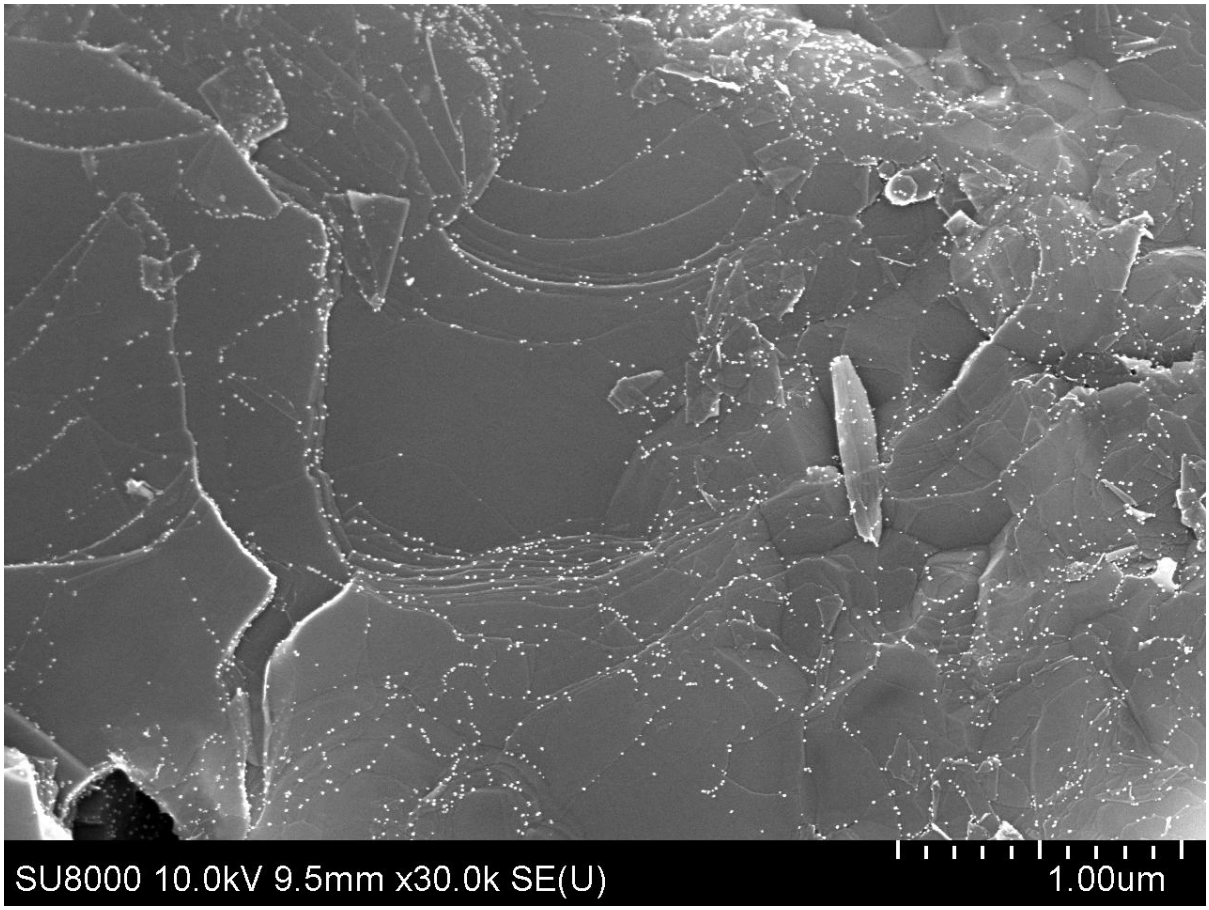

Figure S24. FE-SEM-image of defects mapped by Pd NPs.

2. High resolution images and EDX-elemental mapping

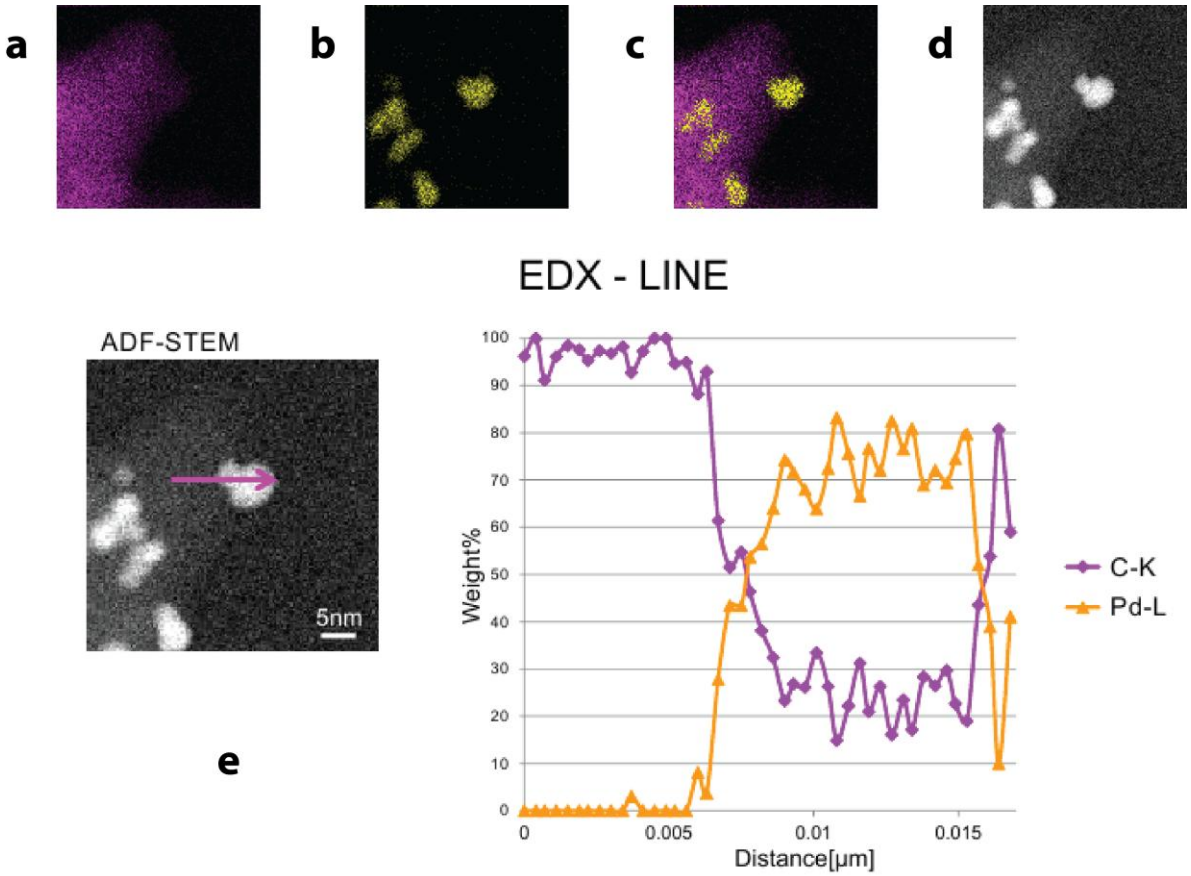

Figure S25. EDX-elemental mapping images of nanoparticles on edge of carbon lattice, carbon is shown in purple, palladium is shown in yellow. **a**, map of carbon distribution. **b**, map of palladium distribution. **c**, map of distribution of carbon and palladium. **d**, ADF-STEM image. **e**, profile of elements distribution, orange line is a weight percent of palladium, purple line is a weight percent of carbon.

3. Computational section

Several issues should be addressed considering the validity of the used modeling approach. Since only Γ-point is accounted in the present implementation of GPW method, inconsistencies may arise due to the gapless electronic structure of the sp^2-carbon systems. It has been shown recently that Γ-point-only calculations may account for the gapless nature of sp^2-carbon systems, particularly, *pristine* graphene, graphene nanoribbons (GNRs) and carbon nanotubes, if the supercell is chosen properly [1]. The pristine sheets and the models of steppings on graphene surface (that include GNRs) were chosen accordingly to this method. For example one-layer graphene model of the same scale than the used in the present study two layer model has the "gap" of 0.01 eV.

Secondly, it may be questionable whether the PBE-D3 method accurately describes Pd_2-graphene interaction. Hobza and co-workers [2], found that adsorption energies of Pd_2 calculated at PBE/PAW level of theory are significantly less exothermic than those calculated at the more accurate vdW+EE/PAW level (26-32 kcal/mol *vs.* 39-43 kcal/mol correspondingly). We have obtained absolute adsorption energy of Pd_2 on pristine graphene equal to 47 kcal/mol which is more exothermic than the accurate values predicted by Hobza and co-workers (39-43 kcal/mol). However this may be attributed to the fact that we used two-layer model of graphene instead of one-layer model as in the paper by Hobza and co-workers thus dispersion attraction to the subsurface graphene layer presents in our system.

Konh-Sham self-consistent field (KS-SCF) procedure with "ATOMIC" guess and Broyden mixing converged to non-spin-polarized states in most cases. Thus we used diagonalization with DIIS procedure to converge Kohn-Sham wavefunction in pre-optimized model systems and, if the systems were predicted to be spin-polarized, the geometry was finally optimized with Broyden mixing during KS-SCF procedure and the DIIS-optimized wavefunction as the *initial guess*, thus obtaining spin-polarized ground state with optimized geometry. The effect may be very significant for systems with dangling bonds, e.g. in the case of Zigzag-uncapped model system (three dangling bonds) geometry optimization with Broyden mixing during KS-SCF converged to an artificial singlet state with half-integer spin-alpha and spin-beta populations that had 27 kcal/mol higher total energy than the spin-polarized one obtained by geometry optimization with DIIS-obtained initial guess. Unfortunately, the geometry optimizations with DIIS exclusively during the wavefunction relaxation did not converge.

Among the systems with point defects only SV-defected graphene has spin-polarized ground state. Notably, all systems with SV-defected graphene become non-spin polarized upon adsorption of Pd_2. The system with grain boundary defect and the stepping with H-terminated armchair edges were also predicted to be non-spin-polarized. Most other systems with steppings containing uncapped C-atoms or steppings with H- or O-terminated zigzag edges were found to be spin polarized.

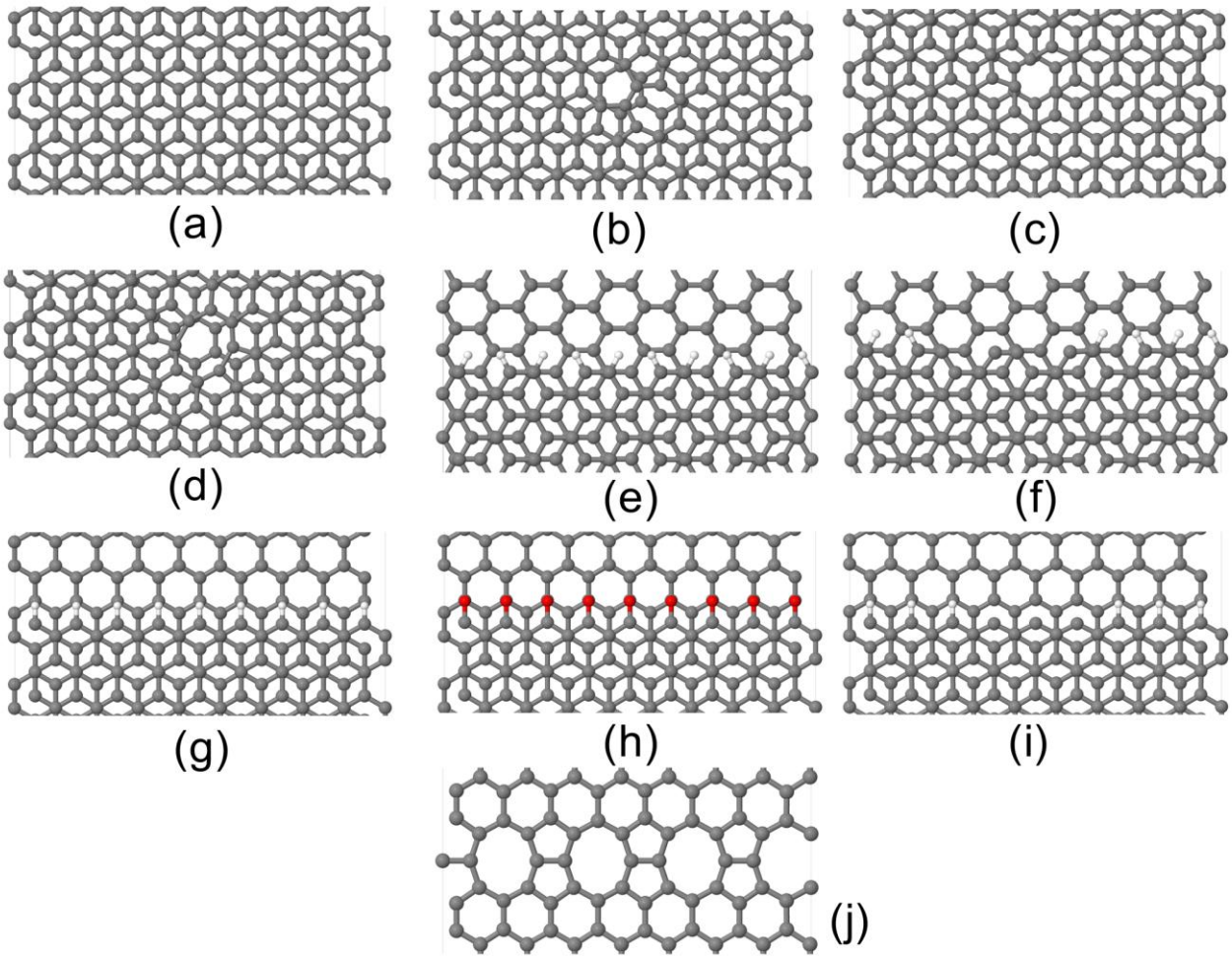

Figure S26. The considered models of structural defects in graphene: (a) pristine two-layer graphene included for comparison; (b) Stone-Wales-type defect; (c) reconstructed single vacancy; (d) reconstructed (5-8-5) double vacancy; (e) stepping with H-terminated armchair edge; (f) stepping with partially uncapped armchair edge; (g) stepping with H-terminated zigzag edge; (h) stepping with O-terminated zigzag edge; (i) stepping with partially uncapped zigzag edge; (j) model of grain boundary. The carbon atoms are marked with gray, oxygen atoms are marked with red and hydrogen atoms are white.

Table S1. Adsorption energies of Pd_2 on pristine and defected graphene calculated at PBE-D3-GPW level of theory. See Computational procedures in Experimental Section for the detailed description of the used computational parameters.

Line number	Adsorbate and adsorption complex configuration	E_{ads} (Pd_2), kcal/mol
	Pristine two-layer graphene	
1	Pristine_1	-48
2	Pristine_2	-50
	Grain boundary	
3	GB_1	-66
4	GB_2	-67
5	GB_3	-61
	Stone-Wales-type defect	
6	SW_1	-72
7	SW_2	-67
	Stepping with H-terminated armchair edge	
8	Armchair-H_1	-58
9	Armchair-H_2	-60
10	Armchair-H_3	-75
11	Armchair-H_4	-73
	Stepping with H-terminated zigzag edge	
12	Zigzag-H_1	-58
13	Zigzag-H_2	-90
14	Zigzag-H_3	-43
15	Zigzag-H_4	-66
	Stepping with O-terminated zigzag edge	
16	Zigzag-O_1	-101
17	Zigzag-O_2	-85
18	Zigzag-O_3	-105
	Double vacancy	
19	DV_1	-68
20	DV_2	-112
21	DV_3	-63
22	DV_4	-71
23	DV_5	-66
	Single-vacancy	
24	SV_1	-128
25	SV_2	-142

	Stepping with uncapped zigzag edge	
26	Zigzag-uncapped_1	-175
	Stepping with uncapped armchair edge	
27	Armchair-uncapped_1	-214
28	Armchair-uncapped_2	-147

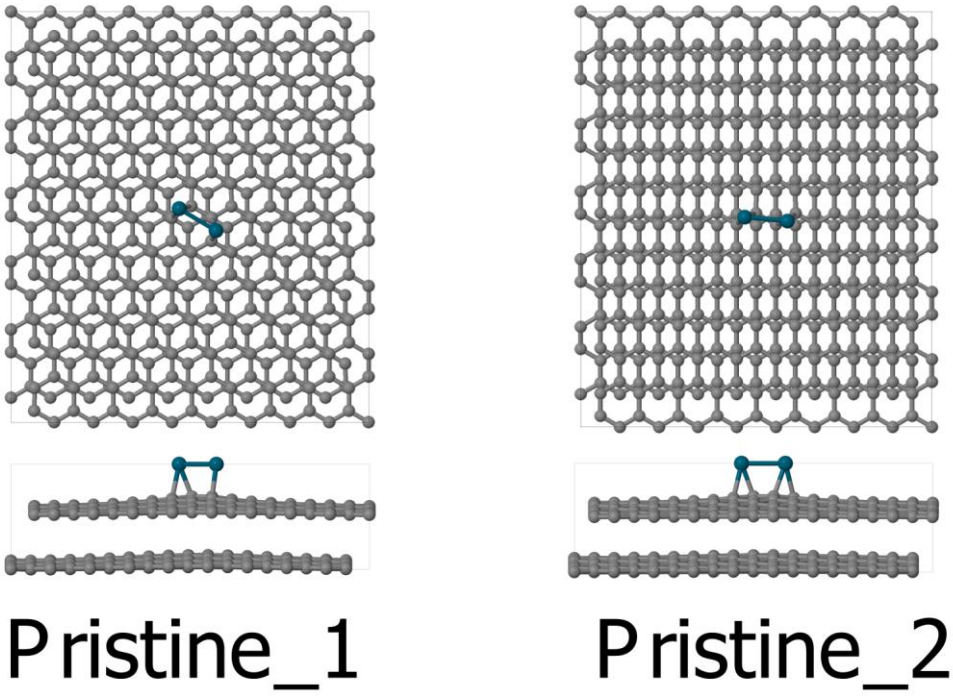

Figure S27. Models of Pd_2 adsorption complexes on pristine graphene. See Table S1 for corresponding adsorption energies.

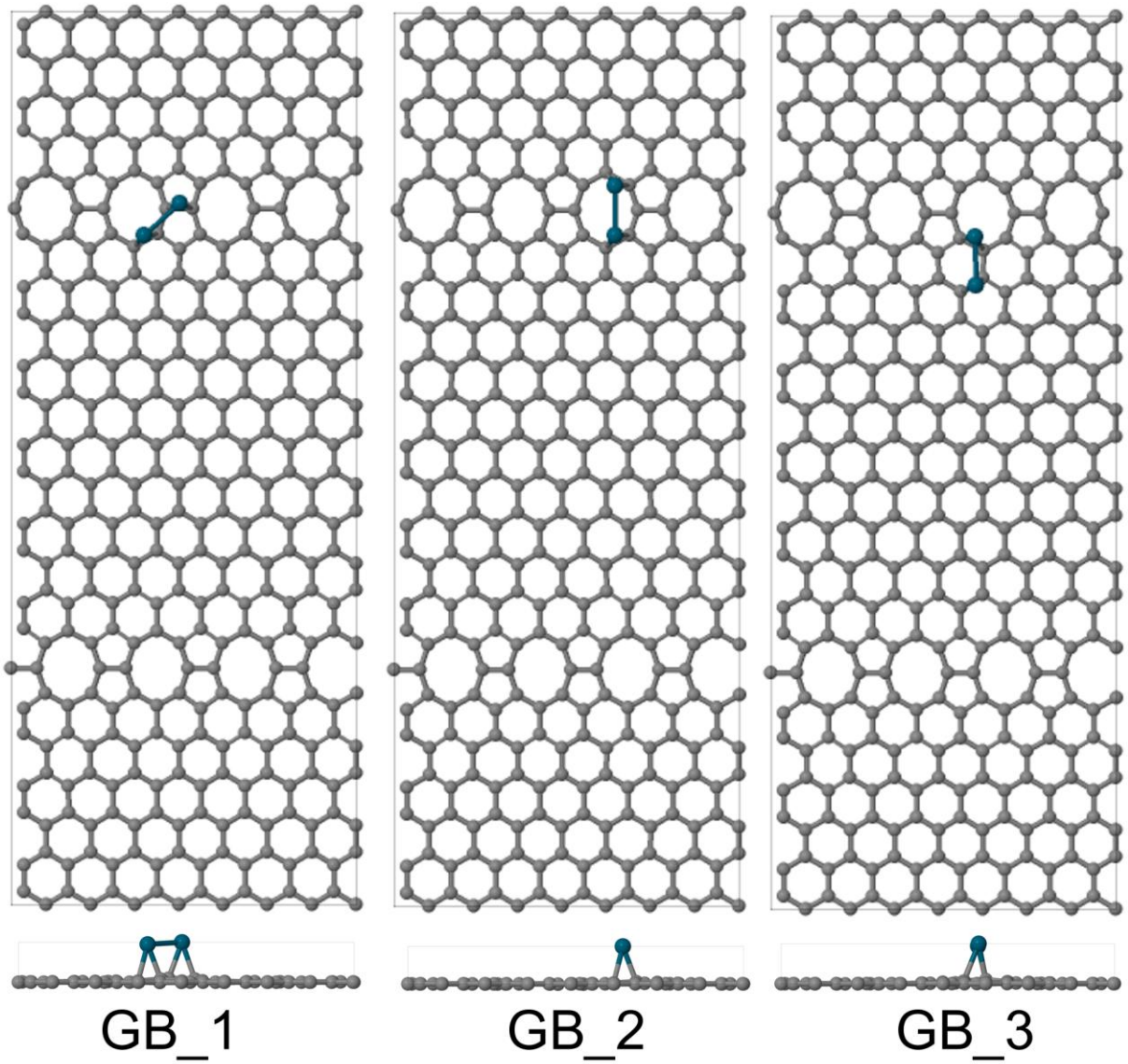

Figure S28. Models of Pd_2 adsorption complexes on grain boundary defect. See Table S1 for corresponding adsorption energies.

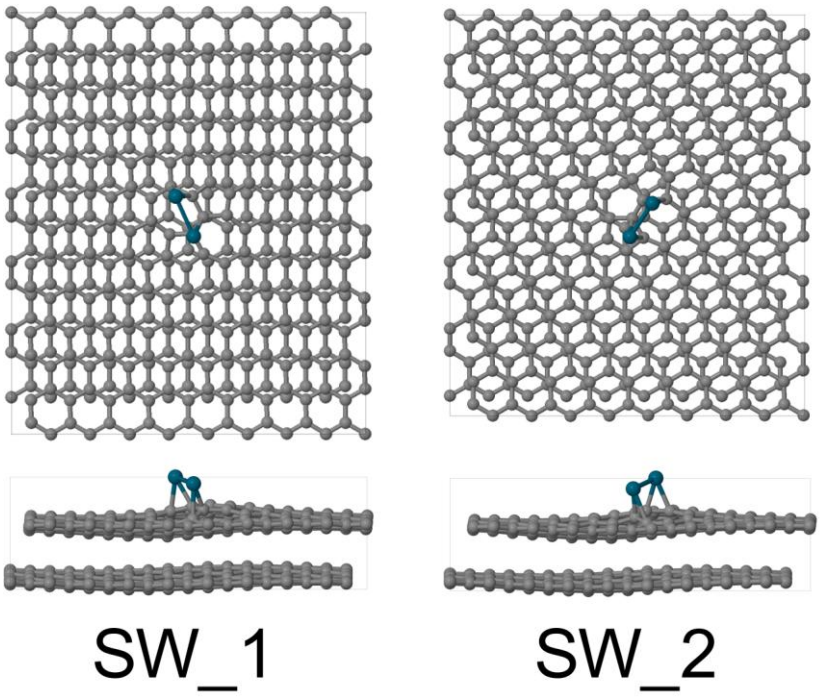

Figure S29. Models of Pd_2 adsorption complexes on Stone-Wales-type defect. See Table S1 for corresponding adsorption energies.

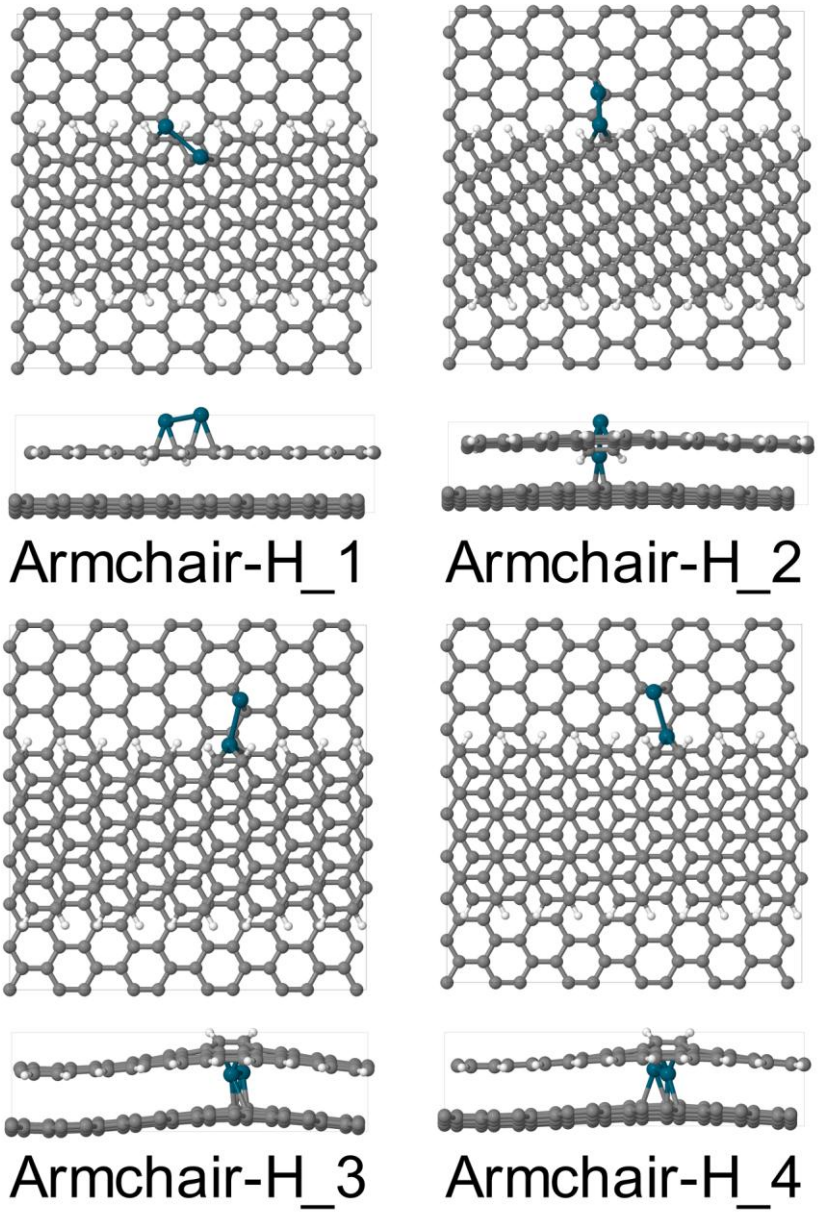

Figure S30. Models of Pd_2 adsorption complexes on stepping with H-terminated armchair edge. See Table S1 for corresponding adsorption energies.

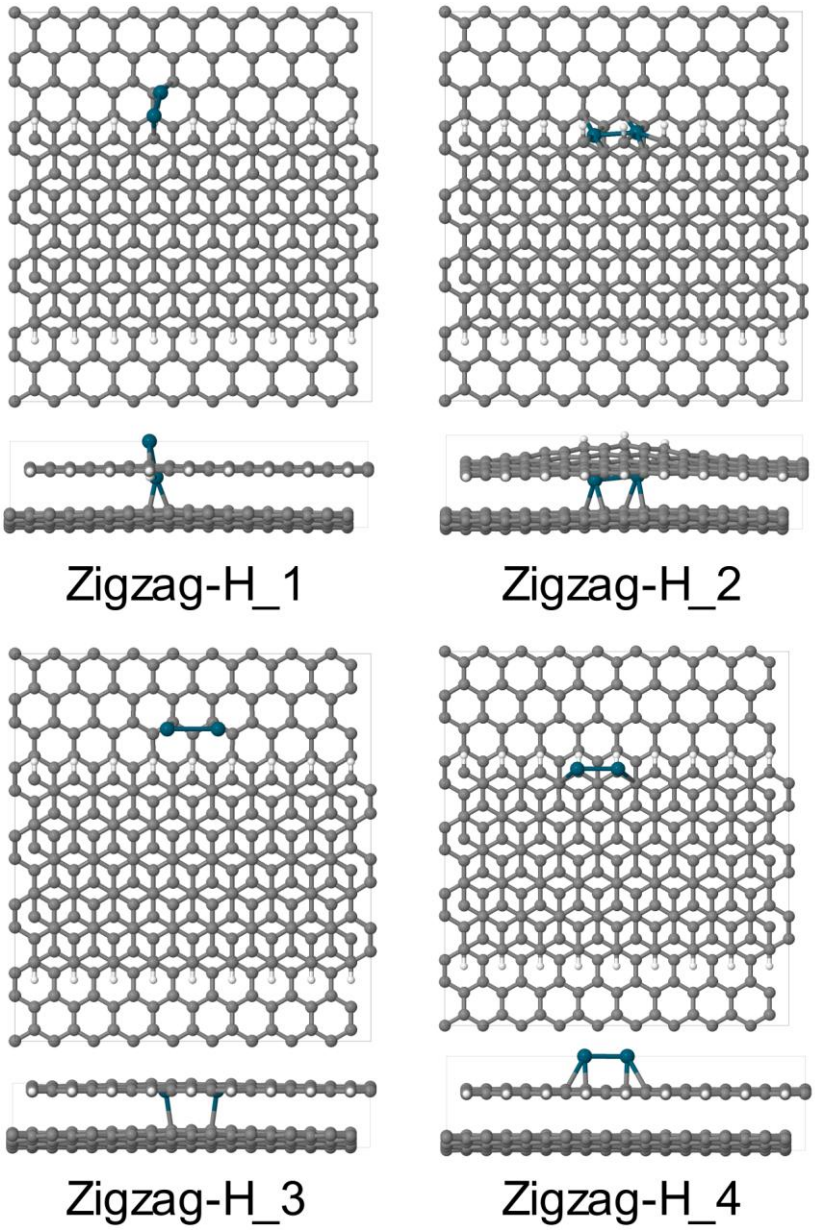

Figure S31. Models of Pd_2 adsorption complexes on stepping with H-terminated zigzag edge. See Table S1 for corresponding adsorption energies.

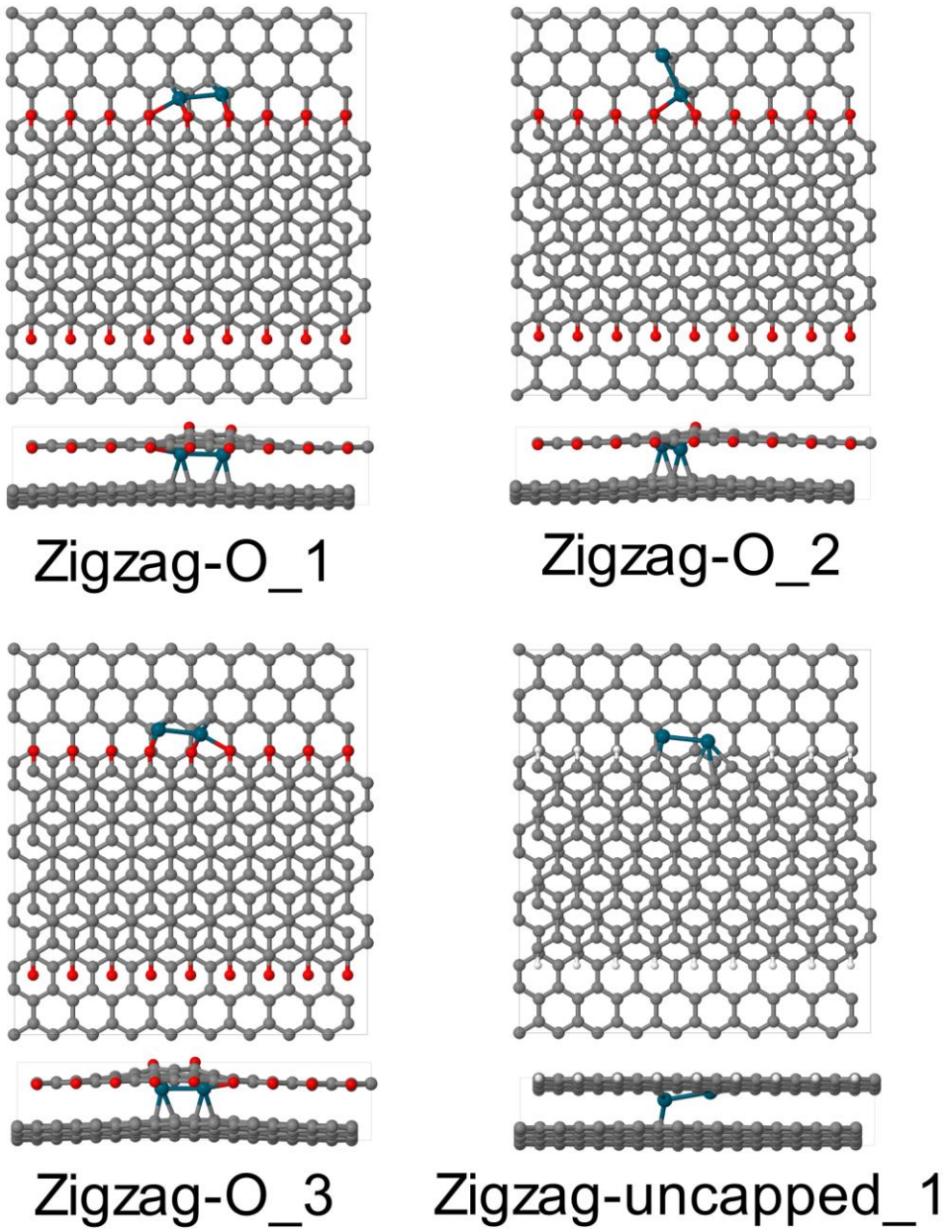

Figure S32. Models of Pd_2 adsorption complexes on stepping with O-terminated zigzag edge and partially uncapped zigzag edge. See Table S1 for corresponding adsorption energies.

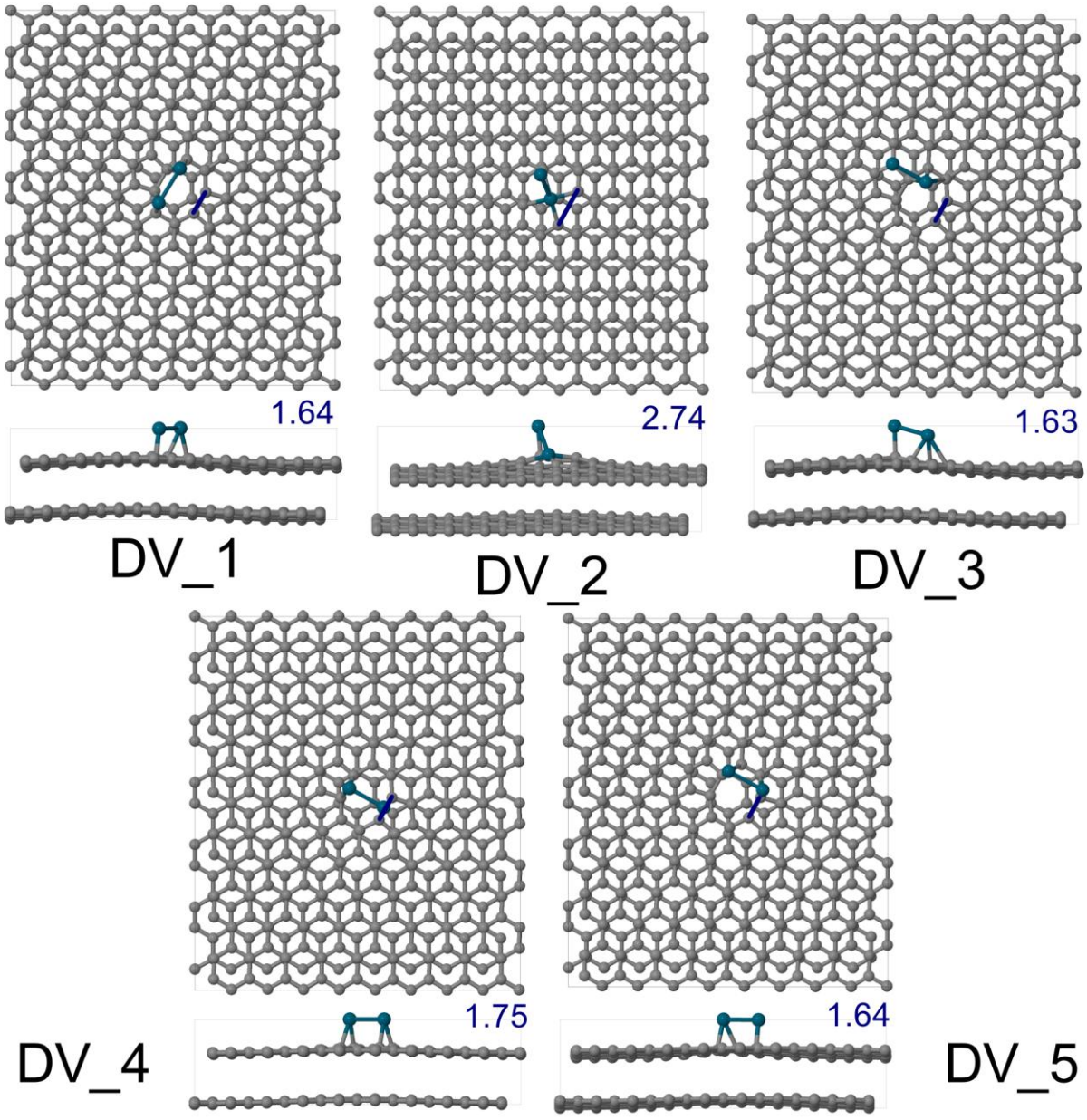

Figure S33. Models of Pd_2 adsorption complexes on double vacancy defect. See Table S1 for corresponding adsorption energies. The distances between two carbon atoms incorporated into fused C-5 and C-8 rings of the defect are marked with blue and given in Å below the top views of the model systems. The same C-C-distance in freestanding two-layer DV-graphene system is 1.63 Å.

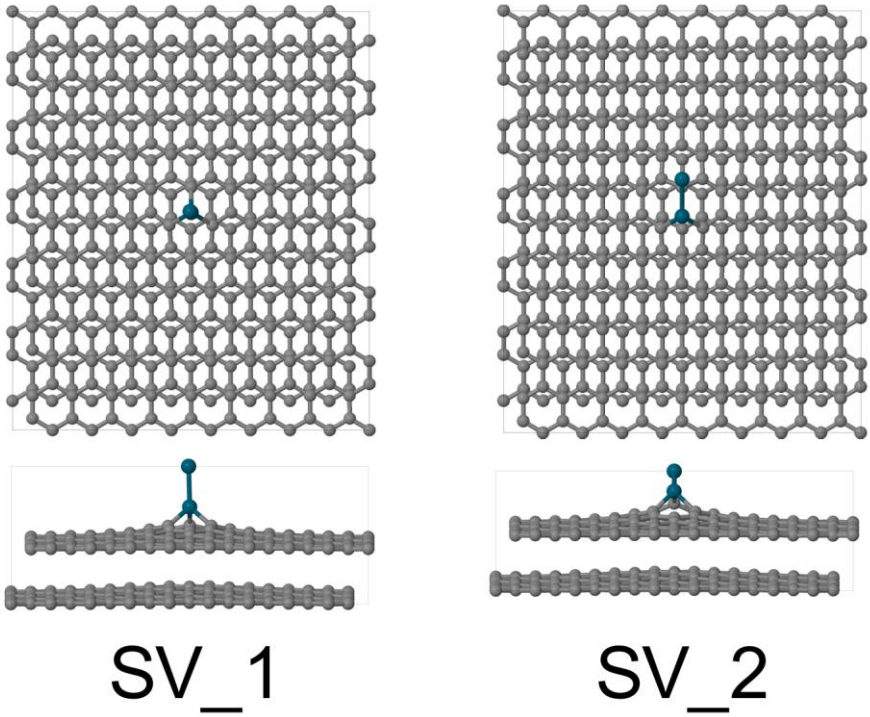

Figure S34. Models of Pd_2 adsorption complexes on single vacancy defect. See Table S1 for corresponding adsorption energies.

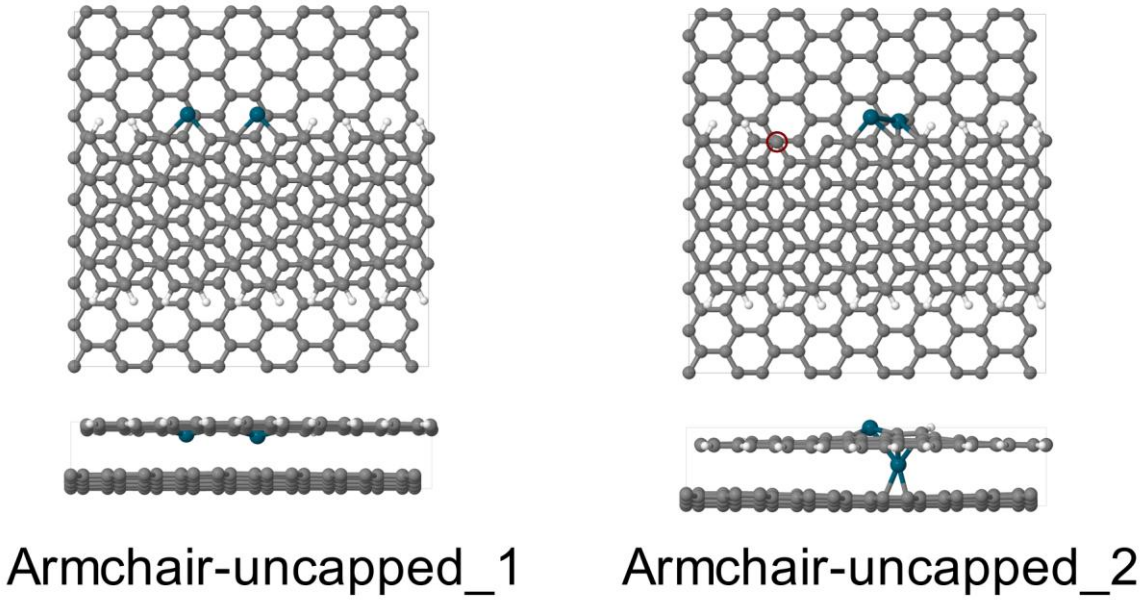

Figure S35. Models of Pd_2 adsorption complexes on stepping with partially uncapped armchair edges. See Table S1 for corresponding adsorption energies. Carbon atom with unpaired electron in the Armchair-uncapped_2 structure is marked with a red circle.

REFERENCES

[1] Ghorbani-Asl, M.; Juarez-Mosqueda, R.; Kuc, A.; Heine, T. *J. Chem. Theory Comp*. **2012,** *8*, 2888-2895, [10.1021/ct3003496].
[2] Granatier, J.; Lazar, P.; Prucek, R; Šafářová, K.; Zbořil, R.; Otyepka, M.; Hobza, P. *J. Phys. Chem. C* **2012** *116*, 14151-14162, [10.1021/jp3030733].